Xiao *et al. Soft Sci* 2023;3:11
**DOI:** 10.20517/ss.2023.03

**Soft Science**

**Review Article**

**Open Access**

Check for updates

# Recent advances in the design, fabrication, actuation mechanisms and applications of liquid crystal elastomers

**Yue Xiao[1,2,#], Jun Wu[1,2,#], Yihui Zhang[1,2,*]**

[1]AML, Department of Engineering Mechanics, Tsinghua University, Beijing 100084, China.
[2]Laboratory of Flexible Electronics Technology, Tsinghua University, Beijing 100084, China.
[#]Authors contributed equally.

[*]**Correspondence to:** Prof. Yihui Zhang, AML, Department of Engineering Mechanics, Tsinghua University, No. 30 Shuangqing Road, Beijing 100084, China. E-mail: yihuizhang@tsinghua.edu.cn

**How to cite this article:** Xiao Y, Wu J, Zhang Y. Recent advances in the design, fabrication, actuation mechanisms and applications of liquid crystal elastomers. *Soft Sci* 2023;3:xx. https://dx.doi.org/10.20517/ss.2023.03

**Received:** 30 Jan 2023 **First Decision:** 23 Feb 2023 **Revised:** 20 Mar 2023 **Accepted:** 29 Mar 2023 **Published:** 15 Apr 2023

**Academic Editor:** Dae-Hyeong Kim **Copy Editor:** Ke-Cui Yang **Production Editor:** Ke-Cui Yang

## Abstract

Liquid crystal elastomers (LCEs), as an intriguing class of soft active materials, exhibit excellent actuation performances and biocompatible properties, as well as a high degree of design flexibility, which have been of increasing interest in many disciplines. This review summarizes recent developments in this inspiring area, providing an overview of fabrication methods, design schemes, actuation mechanisms, and diverse applications of LCEs. Firstly, two-stage and one-pot synthesis methods, as well as emerging fabrication techniques (e.g., 3D/4D printing and top-down microfabrication techniques) are introduced. Secondly, the design and actuation mechanisms are discussed according to the different types of stimuli (e.g., heat, light, and electric/magnetic fields, among others). Thirdly, the representative applications are summarized, including soft robotics, temperature/strain sensors, biomedical devices, stretchable displays, and smart textiles. Finally, outlooks on the scientific challenges and open opportunities are provided.

**Keywords:** Liquid crystal elastomers, fabrication, actuation, stimuli, applications

## INTRODUCTION

In the recent decade, soft active materials[1-3] have been a focusing topic in both the academia and industrial

areas, owing to the increasing demand for flexibility, reliability, controllability, and intelligence in next-generation actuation devices[4-12]. Liquid crystal elastomers (LCEs) are a class of attractive soft active polymers, with excellent actuation capabilities under various types of stimuli, e.g., heat, light[13,14], and electric field, among others. Crosslinked by rigid liquid crystal (LC) mesogens and flexible polymer networks, LCEs show many outstanding mechanical performances, such as rubber elasticity[4,15,16], shape memory effect[17-19], and high uniaxial/biaxial actuation strains[16]. The alignment of the mesogens in the LCEs could be orientated along a specific direction by forces[20] and various external fields[21,22], allowing their transformation into the monodomain state. Moreover, the alignment could be reoriented by physical[19,23,24] or chemical[25] stimuli, causing a phase transition from the monodomain state to the polydomain state[4]. According to the types of LCs, LCEs could be classified into three categories, including nematic[26] and smectic[27] LCEs, with different functions and actuation capabilities. To date, various fabrication and alignment methods of LCEs have been reported[28-30], motivating the applications of LCEs in soft robotics[31], sensors[32], and biomedical devices[33], among others[34]. While the fabrication /alignment methods and thermal/optical actuation capabilities of LCEs have been discussed thoroughly in several recent reviews, an overview of various design schemes, actuation strategies, and their wide-ranging applications is still lacking.

In this review, we focus on recent advances in the fundamental and applied studies of LCEs, covering the fabrication methods, design schemes, actuation mechanisms, and diverse applications, as illustrated in Figure 1. The second section presents a brief introduction to the fabrication and alignment methods of LCEs, as these aspects have been addressed in detail by several comprehensive reviews[4,28,30,31,35-37]. The third section summarizes mechanical responses and actuation strategies triggered by various types of stimuli (e.g., heat, light, electric/magnetic field, swelling, etc.). The fourth section discusses recent advances toward practical applications, including soft robotics, temperature/strain sensors, and biomedical devices, among others. Finally, perspectives on scientific challenges and opportunities for future research are provided.

## FABRICATION OF LCES

Currently, two main types of fabrication methods have been used to fabricate LCEs. The most widely adopted method is the two-stage thiol-acrylate Michael addition and photopolymerization (TAMAP) reaction, originally proposed by Küpfer and Finkelmann[55] and later on, developed by Yakacki *et al.* [Figure 2A][56]. In the first stage, a weakly crosslinked LCE is prepared and then stretched under a mechanical loading for the alignment of LC mesogens. In the second stage, the weakly crosslinked LCE is exposed to UV light to fix the temporary alignment. When the fixed alignment is at the monodomain state, the LCE possesses a two-way shape memory effect, which could be used for reversible actuation. Based on this method, 3D/4D printing techniques were developed, where the shear stress was usually exploited for the alignment [Figure 2B][57]. The mesogens could be aligned along the printing path during the high-operating-temperature direct ink writing (HOT-DIW) process of viscous inks. Based on these 3D/4D printing techniques, the LCE architectures could be programmed on demand to allow reversible 2D-to-3D deformations when heated from room temperature to the nematic-isotropic transition temperature. Additionally, the shear stresses have also been used in the fiber electrospinning[29,58], drawing[54], or microfluidic aligning[59,60] process, aiming to fabricate monodomain LCE fibers. As an example, Roach *et al.* drew very long (~1.5 m) fibers through a nozzle onto a rotating mandrel [Figure 2C][54]. Such fibers offer excellent mechanical performances (2 MPa stiffness, 51% actuation strain, and over 100% failure strain). In Figure 2D, Ohm *et al.* used a microfluidic setup to inject the LCE solution into a co-flowing stream of silicone oil and fabricated highly oriented fibers[59].

The other mainstream method is the one-pot synthesis method, in which the mesogens in the former solution are aligned before the crosslinking reaction and curing process. In Figure 2E, Zeng *et al.*[61] used a

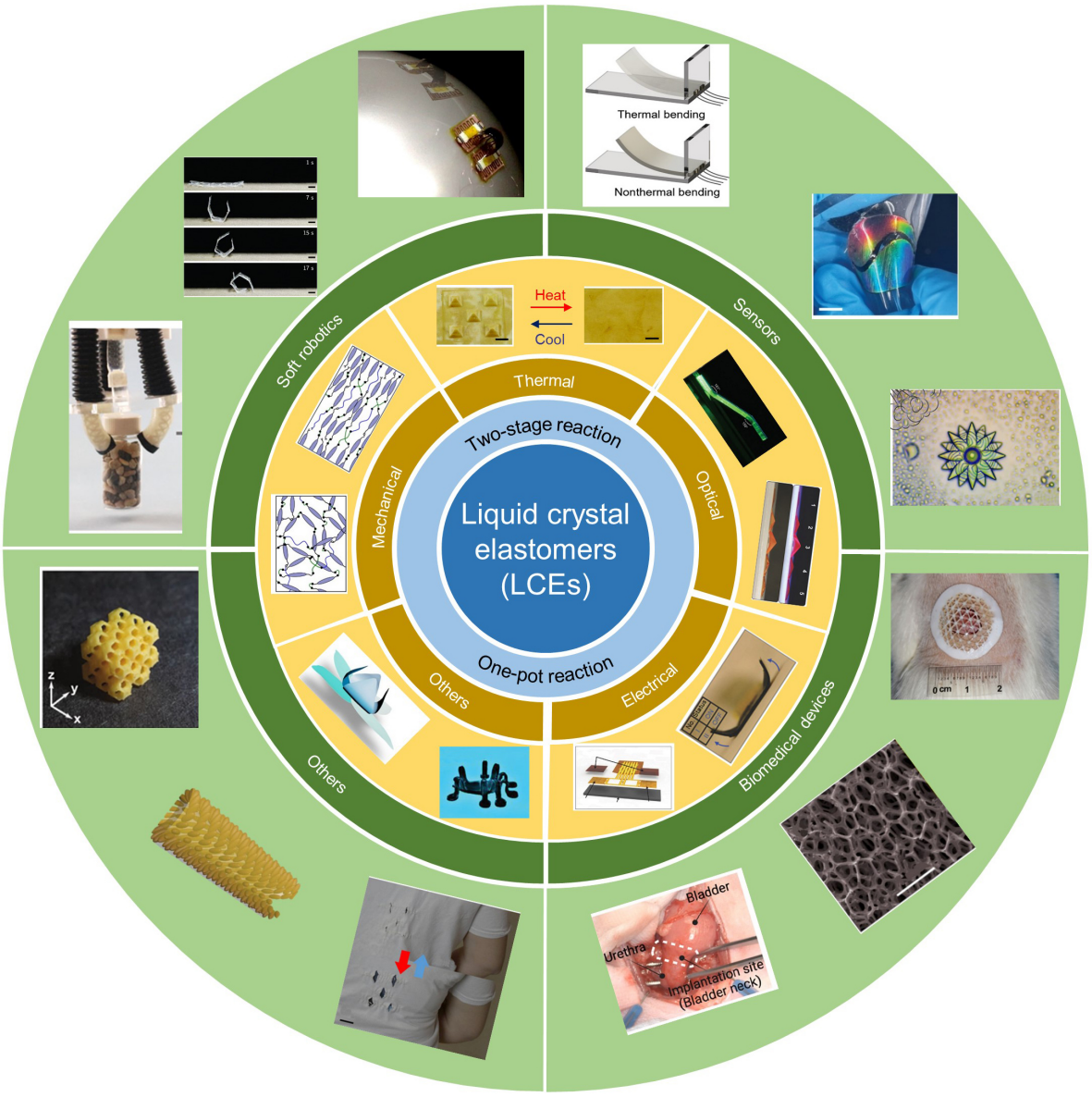


**Figure 1.** Summary of the review on liquid crystal elastomers (LCEs). The main synthesis methods include the two-stage and one-pot crosslinking reaction methods. With strategic material designs, LCEs could be responsive to a variety of external stimuli, such as heat, light, and electric/magnetic field, among others. Owing to their outstanding actuation performances, LCEs can be adopted for applications in a wide range of areas, including soft robotics, sensors, and biomedical devices, among others. Image for "mechaninical". The stress and strain curves. Reproduced with permission[38,39]. Copyright 2020, Wiley Periodicals LLC. Image for "thermal". Reproduced with permission[23]. Copyright 2005, The Royal Society of Chemistry. Image for "optical". The upside image: Reproduced with permission[40]. Copyright 2019 WILEY-VCH. The downside image: Reproduced with permission[41]. Copyright 2016, WILEY-VCH. Image for "electric". Reproduce with permission[42]. Copyright 2018, WILEY-VCH. Image for "others". The left-side image. Reproduced with permission[43]. Copyright 2022, American Association for the Advancement of Science. The right-side image. Reproduced with permission[44]. Copyright 2021, Wiley-VCH. The image in soft robotics from left to right. Reproduced with permission[45]. Reproduced with permission[46]. Copyright 2019, American Association for the Advancement of Science. Copyright 2019, American Association for the Advancement of Science. Reproduced with permission[47]. Copyright 2022, National Academy of Science. The sensor from left to right. Reproduced with permission[14]. Copyright 2021, American Association for the Advancement of Science. Reproduced with permission[48]. Copyright 2022, Wiley-VCH GmbH. Reproduced with permission[49]. Copyright 2020, American Chemical Society. The biomedical device from left to right. Reproduced with permission[50]. Copyright 2022, Elsevier. Reproduced with permission[51]. Copyright 2016, American Chemical Society. Reproduced with permission[52]. Copyright 2021, WILEY-VCH. The other device from left to right. Reproduced with permission[12]. Copyright 2020, WILEY-VCH. Reproduced with permission[53]. Copyright 2021, WILEY-VCH. Reproduced with permission[54]. Copyright 2019, American Chemical Society.

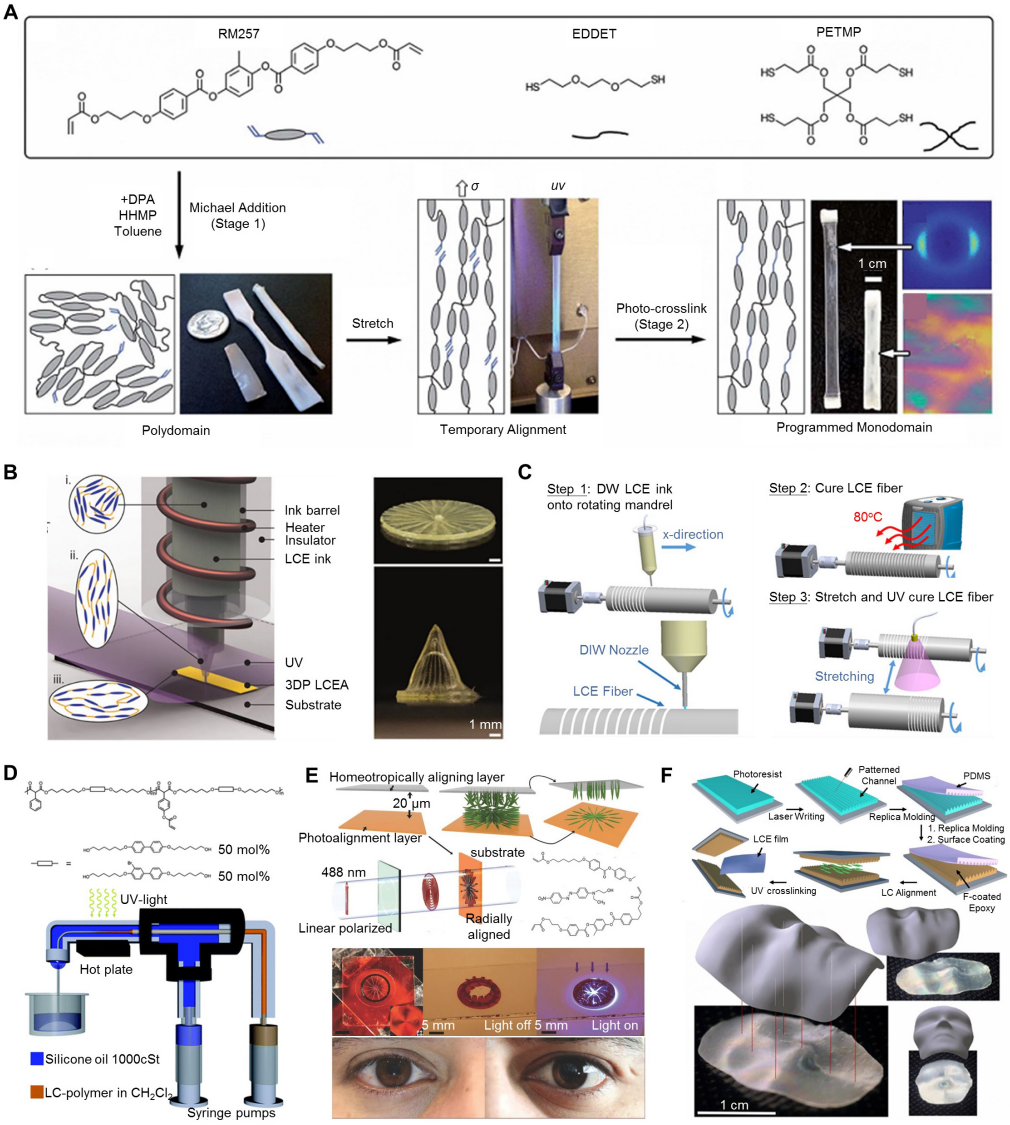


**Figure 2.** Synthesis and alignment methods of LCEs. (A) Two-stage thiol-acrylate Michael addition and photopolymerization reaction. Scale bar, 1 cm. Reproduced with permission[56]. Copyright 2011, RSC advances; (B) 3D printing methods for creating LCE structures with complex patterns. Scale bars, 1 mm. Reproduced with permission[57]. Copyright 2018, WILEY-VCH; (C) schematic illustration of the drawing process for producing LCE fibers. Reproduced with permission[54]. Copyright 2019, Royal Society of Chemistry; (D) schematic illustration of the microfluidic method for producing LCE fibers. Reproduced with permission[59]. Copyright 2005, Royal Society of Chemistry; (E) one-pot crosslink reaction by surface treatment for the alignment at local regions, which was used for the fabrication of a LCE iris. Scale bars, 5 mm. Reproduced with permission[61]. Copyright 2017, WILEY-VCH; (F) top-down microfabrication techniques for one-pot fabrication of LCE sheets with a programmable alignment. The deformed configuration is like a human face. Scale bar, 1 cm. Reproduced with permission[62]. Copyright 2018, National Academy of Sciences.

surface-enforced strategy to fabricate a LCE iris. At the upper surface, the LC mesogens are in a homeotropic alignment; and at the bottom surface, an azobenzene-based photoalignment layer is painted such that the mesogens could be aligned by the polarization of the incident light. Similar to the natural iris, the iris-like device could gradually close with increasing the light intensity, thereby reducing the light transmission. In Figure 2F, Aharoni *et al.*[62] used advanced top-down microfabrication techniques to produce flat LCE sheets with programmable patterns, which allowed the formation of controlled 3D shapes above the nematic-isotropic transition temperature, such as the human face.

As the most widely adopted synthesis method, the two-stage synthesis method shows advantages in the fabrication of monodomain LCEs with feature sizes[45,63]. The alignment of the LCEs is usually implemented using mechanical stretching and other relevant techniques (e.g., 4D printing and electrospinning), whose pattern precisions are usually above 20 μm[47]. Therefore, the complex alignment pattern of the LC mesogens in a small local region (~10 μm) remains a challenge for the two-stage synthesis method. The one-pot synthesis method is usually adopted to fabricate thin LCE films (e.g., 10-50 μm in thickness) with complex alignment patterns[64,65]. However, the LCEs with large sizes (> 1 cm) are difficult to fabricate using the one-pot synthesis method. Except for the LCEs with regular covalent bonds that are fabricated by the one-pot or two-stage synthesis method, the LCEs with dynamic covalent bonds were initially reported by Pei Z *et al.*[66], based on reversible and dynamic chemistries. Different from the LCEs with regular covalent bonds, the LCEs with dynamic covalent bonds can be reshaped or reprogrammed by mechanical deformations above the topology-freezing transition temperature (i.e., an activation barrier temperature for the fast breaking and reforming of the ester bonds)[67]. Despite the reprogramming capability, the LCEs with dynamic covalent bonds are difficult to be designed with complex patterns in a small local region (~10 μm) because the dynamic exchange reaction for the reprogrammable LCEs needs mechanical stretching, whose precision for the alignment is above 100 μm.

## DESIGN AND ACTUATION MECHANISMS OF LCES

### Mechanical responses

LCEs are composed of LC mesogens (i.e., rod-like molecular segments) connected to a flexible polymer network. Figure 3A shows that the mesogenic groups can be characterized by the type of ordering, such as the ordered (smectic or nematic) phase and the disordered (isotropic) phase[32]. The smectic LC means the molecules are positionally ordered along one direction. The nematic LCEs means that the LCEs molecules are aligned in the same direction, and the nematic LCEs are usually classified further into the fully-enforced alignment (monodomain LCEs) and the macroscopically-unaligned alignment (polydomain LCEs)[38]. The representative micro-structures of LCEs are illustrated in Figure 3B. Meanwhile, LCEs can be divided into the main-chain LCEs (with the mesogen embedded into the backbone of a polymer chain) and the side-chain LCEs (with the mesogen attached to the main chain as side groups), depending on the mesogenic group incorporated methods [Figure 3A][32]. The alignment of LC mesogens is quantitatively described by the average orientation of mesogens, characterized by the director **n**. This order degree of the alignment is defined by the order parameter: *S*. It is noteworthy that the LC alignment and the crosslinking type have a strong impact on the mechanical responses of LCEs.

Generally, the polydomain nematic LCEs can be divided into the isotropic-genesis polydomain nematic LCEs (I-PNLCEs) and nematic-genesis polydomain nematic LCEs (N-PNLCEs) according to the LC phase during crosslinking process[39,68,69]. They both show a relatively linear relationship between applied stress and strain at small strains and a stress plateau at intermediate stress [Figure 3C], which is denoted as soft elasticity (or semisoft elasticity)[70]. The N-PNLCEs possess high modulus and stress plateau than the I-PNLCEs. During the loading process, the director is reoriented to align with the loading direction. When the domains are fully aligned to the loading direction, stiffer stress-strain responses are observed at high strains after the regime of soft elasticity. The monodomain LCE shows an evident anisotropic effect[16]. Specifically, the monodomain LCE offers a rather linear stress-strain response when the loading direction is close to the initial orientation of mesogens. Under the orthogonal-dominated loadings, the stress-strain response shows an apparent soft elasticity and a strain-hardening feature. The anisotropic effect can be well captured by the theoretical modeling considering the director reorientation[16], as evidenced by the agreements with results of the finite element analysis (FEA) in Figure 3D.

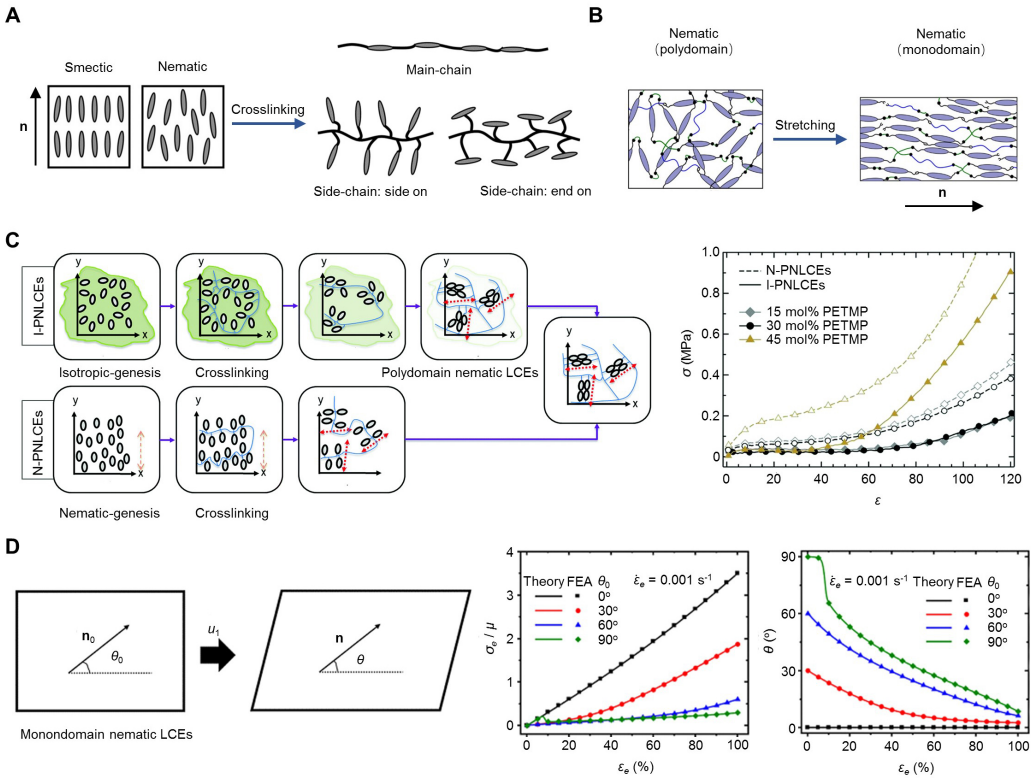


**Figure 3.** Mechanical responses of LCEs. (A) Schematic illustration of various phases and the crosslinking of LC mesogens. Reproduced with permission[32]. Copyright 2010, Wiley-VCH; (B) illustration of the polydomain and monodomain nematic LCEs. Reproduced with permission[38]. Copyright 2020, Wiley Periodicals LLC; (C) nonlinear mechanical responses of polydomain nematic LCEs under uniaxial stretching and the associated evolutions of LC alignments. Reproduced with permission[39]. Copyright 2017, RSC advances; (D) stress-strain curves of the monodomain nematic LCE under different loading directions. Reproduced with permission[16]. Copyright 2021, Wiley-VCH.

Within the broader classification of the LC mesogens, the crosslinking density, the nature of mesogens (nematic or smectic), and the polymer chain conformation play fundamental roles in the mechanical properties of LCEs. The crosslinking density tends to decrease their stretchabilities, as a higher density stiffens the polymer network. Additionally, the crosslinking moieties could cause defects in the network, thereby reducing the chain anisotropy[71,72]. The nature of mesogens affects the stretchability evidently. Usually, the smectic LCEs show a lower stretchability than the nematic LCEs. Deforming and actuating performances are affected by the polymer chain conformation[73]. The stretchability and actuation performances of the main-chain LCEs[74] are more outstanding than the side-chain LCEs, including the end-on and side-on LCEs[75]. As compared to side-chain LCEs[76], the main-chain LCEs present a higher actuation strain[77].

## Thermal actuation

Thermal actuation is the most widely used actuation strategy of LCEs. Upon heating, the monodomain LCEs exhibit a substantial compression parallel to the director vector[17], owing to the nematic-isotropic transition. The thermomechanical behavior of LCEs during the nematic-to-isotropic transition process has been theoretically studied extensively[16,78], which is essential for programming the shape of LCE film, as required in many practical applications.

Historically, Finkelmann *et al.*[55] demonstrated, for the first time, the thermal actuation of LCEs, by preparing a uniaxially aligned monodomain LCE through mechanical alignment. More versatile self-adaptive deformations can be achieved by altering the strategic regions of alignment and their directions. Figure 4A shows that the flat LCE film, when integrated with a non-actuation material, can realize reversible thermal deformations into various 3D shapes, such as tubes, helices, and waves[79]. More precisely-controlled 3D shape morphings can also be achieved[18,23]. Figure 4B shows a disulfide LCE film fabricated by the embossing method. Here, the film is compressed between male and female molds under 100 °C. The disulfide bonds can be cleaved into thiyl radicals at high temperatures, thus temporarily removing the shape change. When the temperature cools down, the disulfide bonds are formed again, thus emerging the embossed pattern. Moreover, the 2D-to-3D shape morphing actuation can be archived by the origami-inspired designs (or the designs inspired by topological defects)[19,80]. A miura-origami-based LCE film[81] is aligned by the azobenzene-based photoalignment method, enabling 100 distinct director orientations in an area of 100 μm by 100 μm. The film can achieve self-folding and unfolding upon heating and cooling. Figure 4C presents a curing-based shape morphing method through 4D-printing techniques, enabling more degrees of design freedom in the fabrication[19]. The patterning precision for the embossing and the azobenzene-based photoalignment methods is ~0.1 mm. Smaller characteristic sizes of LCE structures can be realized through the template-induced alignment technique[62,82,83]. Using this method, LCE films with 1 μm microchannel patterns (or topological defects) can be fabricated. The film has excellent mechanical performances, and the actuation strain can reach ~50%[84]. Moreover, the film can lift over 700 times its own weight[85].

The thermally actuated LCEs were widely used in practical applications because of the simple control and the easy synthesis. However, the nematic-isotropic transition temperature of the LCE with thermal actuation is typically from 70-80 °C[86], thus limiting its applications under room temperature (20-22 °C) or human-body temperature (~37 °C). Recently, research showed that LCEs could be heated by the surrounding body temperature or the human-body temperature[52,87], thus broadening its application in the bio-devices or the drug delivery system. However, the thermally actuated LCEs usually rely on thermal conduction and convection for heating, but the response time (e.g., 10-100 s) is a bit long[88-91]. He Q *et al.*[88] fabricate the water channel inside the LCE film in Figure 4D, and the LCE film is actuated by the heat transferring under the water heating/cooling process. The actuation time for the thermal LCE actuator is ~25 s, and the corresponding cooling time is ~200 s.

### Optical actuation

By the incorporation of nano-phase materials into LCEs, the LCE-based composites can absorb light almost over the wide spectrum range and convert the absorbed light into heat to achieve fast and precise remotely-controlled actuation. The optical actuation methods can be classified into the photothermal method and the photochemical method. The photothermal LCEs transform the absorbed light into heat, which results in macroscopic actuation. The photochemical LCEs rely on the isomerization method, which is a molecular scale motion upon light exposure in a certain range of wavelength.

The photothermal actuation can be realized by incorporating nano-phase materials [e.g., carbon nanotubes (CNTs), graphenes, metal nanoparticles, dyes, and conjugated polymers (CPs)]. Figure 5A shows a LCE/CNT fiber (with a modulus of 40 MPa along the long axis) that offers excellent actuation performances[92]. Its photothermal response time is within 10 s. The LCE/CNT fiber can absorb light almost over a wide spectrum range[93,94]. The LCE can incorporate the RMGO (reduced chemically modified graphene oxide) to convert light to thermal. According to reported experimental results, an actuation temperature of ~ 122 °C and a contraction of 30% can be achieved. The metal nanoparticles (e.g., nano-Au or nano-Ag) can be incorporated into LCEs to enable excellent optical actuation performances and versatile actuation

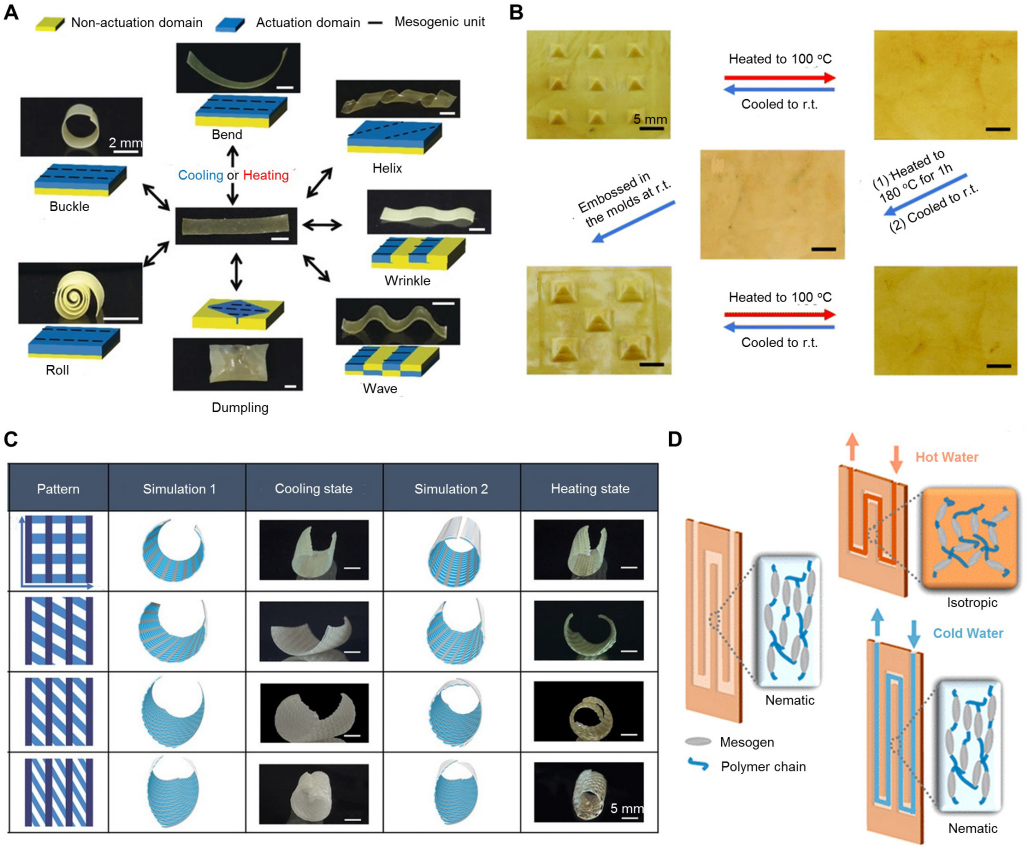


**Figure 4.** Thermal actuation of LCEs. (A) Versatile shape morphing capabilities of LCEs by designing the local LC alignment and incorporating the non-actuation domain. Scale bars, 2 mm. Reproduced with permission[79]. Copyright 2018, WILEY-VCH; (B) illustration of the room-temperature embossing of LCE films, and the reversible actuation of the processed LCE film. Scale bars, 5 mm. Reproduced with permission[23]. Copyright 2005, The Royal Society of Chemistry; (C) FEA simulations and optical images of the LCE actuator composed of two different LCE layers through the 4D-printing method. The light and dark blue regions denote two phases with different light exposure times (9 and 16 s) during the crosslinking process. Scale bars, 5 mm. Reproduced with permission[19]. Copyright 2021 Wiley-VCH GmbH; (D) LCEs with embedded channels, which can be actuated through water heating/cooling. Reproduced with permission[88]. Copyright 2020, American Chemical Society.

modes[95-98]. Figure 5B shows that the LCE incorporating Au nanoparticles (AuNPs) can realize a photo-induced bending[40]. The patterned regions are doped with AuNPs to act as "hinges" in response to waveguided visible light. The bending angles of > 14° can be achieved on the timescale of seconds. Complex bending deformations can be activated through a judicious choice of active placements. Moreover, organic dyes can also serve as photothermal agents[13,99-102]. The organic dyes can absorb quasi-daylight source while maintaining good actuation performances. Furthermore, LCEs show compatibility with CPs responsive to near-infrared light, and therefore, the LCE/CP composites can convert near-infrared light to heat efficiently[103,104]. The CPs are hard to aggregate in the LCE, which thus enables an easy synthesis and processing of LCE/CP composites.

The LCE-based composites capable of absorbing near-infrared light can be used in biomedical applications[105]. Besides, the photothermally responsive LCEs can achieve high-precision spatial control by moderating the light intensity[106,107]. However, the nanoparticles tend to concentrate in LCEs, and such a concentration could evidently stiffen the LCEs, thereby limiting their deformability. For a thick LCE film exposed in the irradiation, a nonuniform temperature rise along the thickness direction could occur, which may induce an undesired bending deformation.

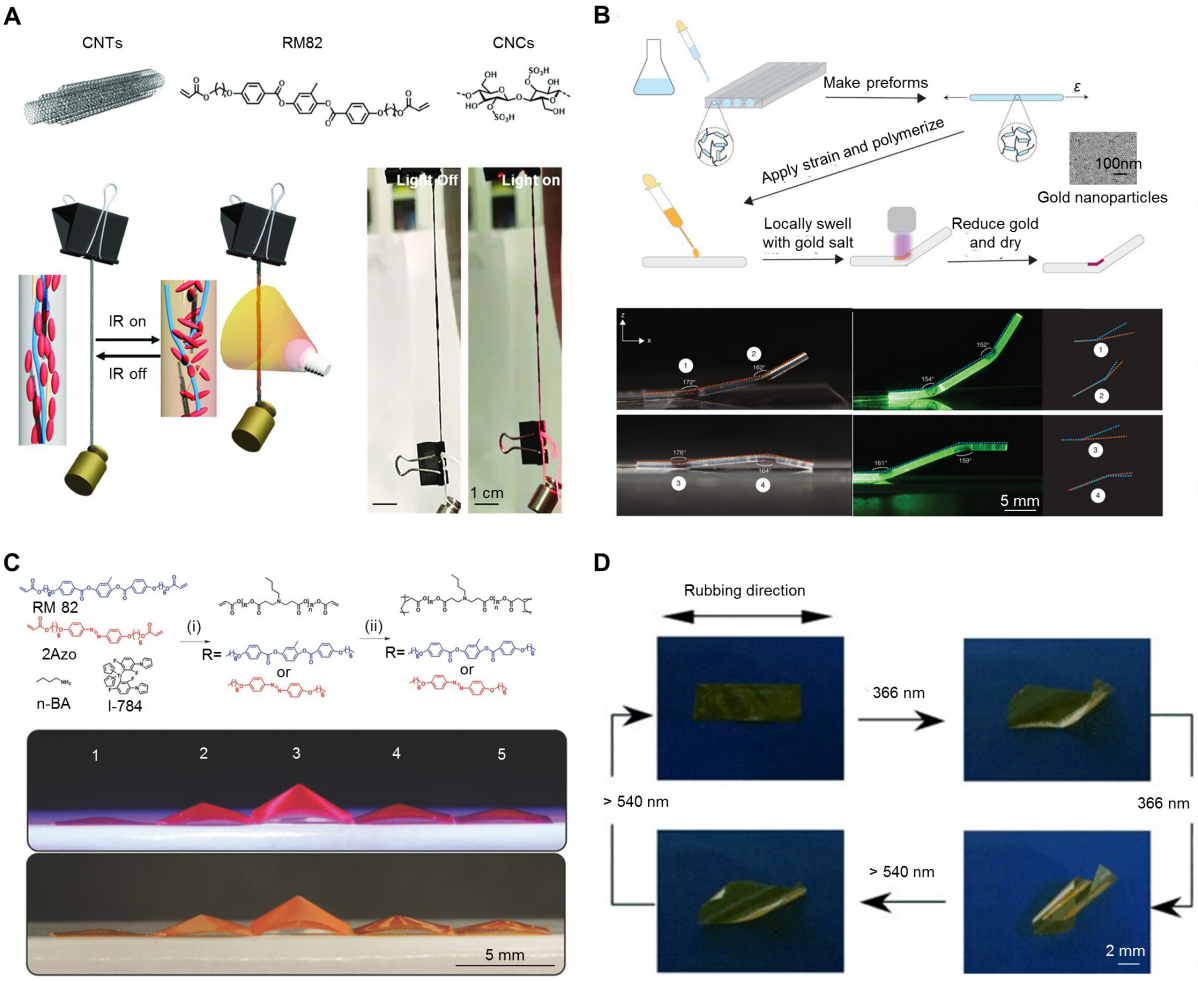


**Figure 5.** Optical actuation of LCEs. (A) Illustration of LCE/CNT composite filaments composed of RM82, CNCs, and CNTs. The bottom panels show the actuation of LCE/CNT using infrared light. Scale bars, 1 cm. Reproduced with permission[92] by CC-YB; (B) LCE-based nanocomposites fabricated by depositing gold solution on the surface of the fiber and locally swelling the fiber before UV exposure. The LCE-based nanocomposite fiber undergoes bending deformations when actuated by waveguided light. Scale bars, 100 nm at the top panel and 5 mm at the bottom. Reproduced with permission[40]. Copyright 2019, WILEY-VCH; (C) illustration of the preparation of the azobenzene-functionalized liquid crystalline elastomers (LCE/azo) by aza-Michael addition reaction and the photopolymerization of the end-capped diacrylate oligomers. The optical images in the bottom panel show the shape morphing of LCE/azo subjected to 365 nm irradiation (100 mW/cm$^{-2}$). Scale bar, 5 mm. Reproduced with permission[41]. Copyright 2016, WILEY-VCH; (D) bending and flattening of the ferroelectric LCE film upon alternate irradiation with UV and visible light at room temperature. Scale bar, 2 mm. Reproduced with permission[112]. Copyright 2007, WILEY-VCH.

The photochemical LCEs incorporate the photosensitive molecules (azobenzene (azo) and its derivatives), which can harness light for actuation. The actuation mechanism for the photochemical LCEs follows the mechanism of thermal isomerization[36,108]. The azo transfers from trans-azobenzene to cis-azobenzene in response to the illumination. When turning the light off, the LCE/azo composite returns to its initial shape due to the thermal back-isomerization. Macroscopically, the LCE/azo composite contracts/elongates when turning the light on/off. Versatile deformation modes can be realized, including, for example, in-plane contraction/expansion[32], topographical deformations[36,109], and bending deformations[110,111]. Figure 5C shows that the LCEs/azo composite undergoes reversible out-of-plane shape changes under irradiation (532 nm wavelength)[41]. Figure 5D demonstrates that the LCEs/azo composites have fast and strong photo-induced actuation performances[112]. The bending deformation took place within 500 ms upon

irradiation by a 366-nm laser beam. The mechanical stress generated by photo-irradiation reached about 220 kPa, similar to the contraction stress of human muscles (~300 kPa).

The optical actuated LCEs can easily achieve the remote control. However, the thickness for the optically actuated LCEs is typically in the range of 10-100 μm[41,113-115]. When the optically actuated LCEs are too thick, the light will be difficult to fully penetrate the opaque LCE, leading to undesired inhomogeneous deformations along the thickness direction. The photothermal LCEs undergo severe temperature change (> 30 °C) upon actuation[106]; thus, the photothermal LCEs are not suitable for biomedical applications. The photochemical LCEs are actuated with a negligible temperature change. However, the photosensitive molecules for preparing the photochemical LCEs are limited because they only include azobenzene (azo) and its derivatives. Furthermore, the photochemical LCEs respond under selected wavelength ranges (320-380 nm and 400-450 nm)[116].

### Electric actuation

The LCEs integrated with the conductive wires[117] or conductive polymer layers[118] can be actuated by resistive heating. Usually, the conductive wires can realize local actuation of LCEs at selective regions. Figure 6A shows free-standing ultrathin (~2.6 μm thick) serpentine-shaped wires attached to the LCE film[42]. The generated Joule heat (~0.237 W) from the wires (under a voltage of 8.2 V) induces 24% shrinkage along the longitudinal direction. He Q *et al.*[45] demonstrated the integration of LCE with conductive wire to fabricate an actuator capable of multi-directional bending under a voltage of 1.5V. In comparison to actuators made of dielectric elastomers[119], the low-voltage actuation of LCE/wires represents an advantage. The conductive layer can also be made from organic materials, such as poly(3,4-ethylenedioxythiophene): poly(styrenesulfonate)[118]. The deformation of the bilayer film reaches 20% actuation strain and 18% $s^{-1}$ strain rate.

Ferroelectric LCEs can be actuated by electricity due to the electroclinic effect[21,120], in which the smectic layer tilts under an electric field. Figure 6B shows the schematic diagram illustrating the electroclinic effect[121]. Ferroelectric LCEs offer a fast actuation, with a response time on the order of 10ms. Ferroelectric LCEs are typically much more rigid than most nematic LCEs. Ferroelectric LCEs act as a strong resistance to the dielectric realigning force, with high electric field strength (e.g., 1.5 $MV{\cdot}m^{-1}$)[21] and low actuation strain (4%).

Composites that integrate LCEs with liquid metals (LMs) through embedded channels[122-124] and vapor[125] can also achieve electrically-induced actuation. Figure 6C shows LCE-based coaxial fibers with LMs in the center[123]. The fiber has a large actuation strain (nearly 50%) upon the Joule heating. Figure 6D shows the LM vapor trapped in the LCE network[125]. Under the actuation through Joule heating, LCEs/LM can be actuated at rates faster than 2 Hz, and cycled to 50% reversible strain by 15,000 times at 0.007 Hz (and 2.5% reversible strain by > 100,000 times at 1 Hz) while retaining > 90% of its original actuation strain.

Based on the customized circuit pattern, the LCEs with electric actuation could be easily controlled to achieve complex shape transformation through strategic local deformations. The speed of the electric actuation is faster than that of the thermal conduction and convection, with the response time as low as ~0.01 s[126]. Compared with the optically actuated LCEs, the local deformation of the electrically actuated LCEs could be controlled more precisely by adjusting the voltage. However, excessive electric heating is very common to induce material failure, i.e., the delamination between the LCEs and wires/polymer layers[125]. It is difficult to fabricate a miniatured actuator by the integrated LCEs with the LMs because the size of the integrated LCEs is around a millimeter scale.

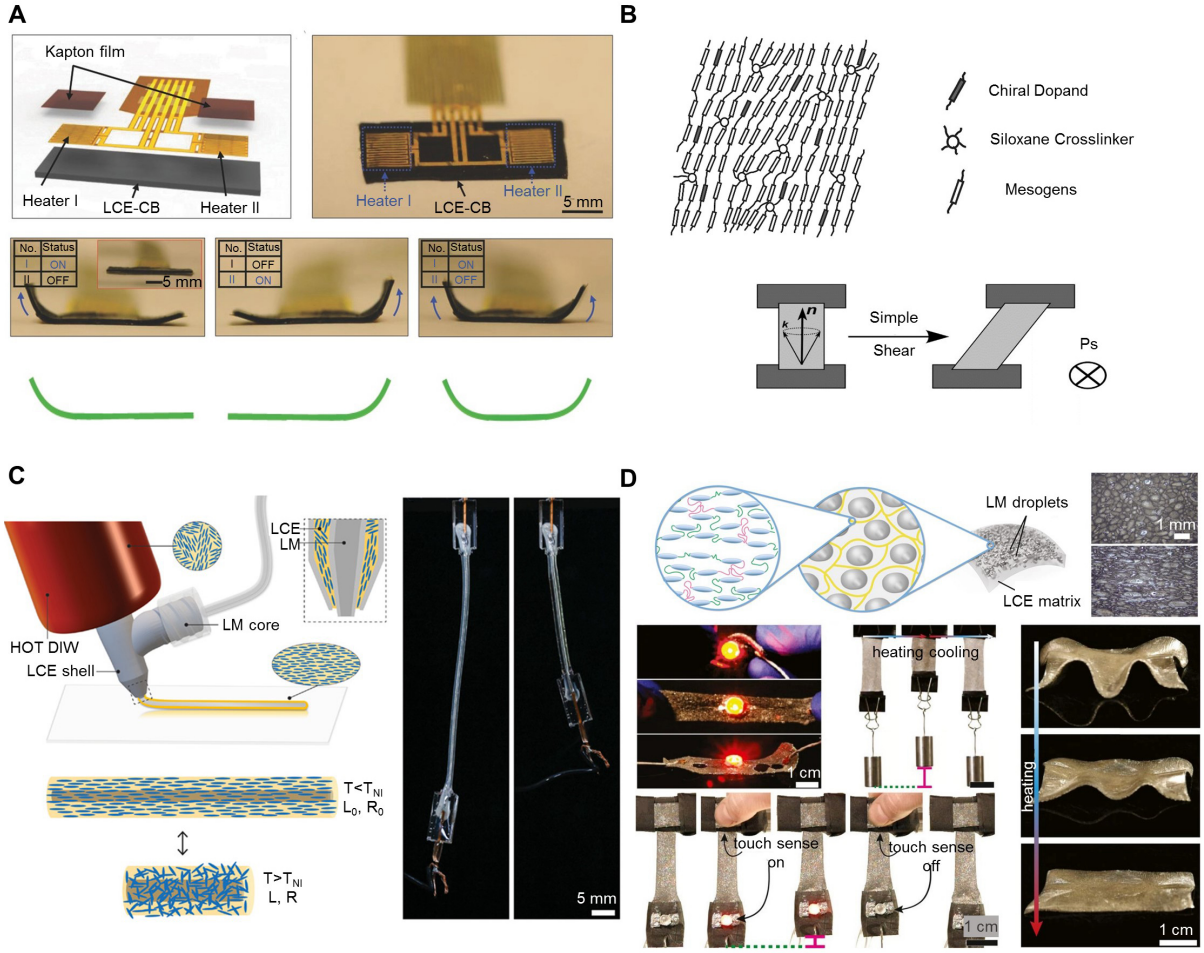


**Figure 6.** Electric actuation of LCEs. (A) Local actuation realized by integrated conductive wires. Scale bar, 5 mm. Reproduced with permission[42]. Copyright 2018, WILEY-VCH; (B) a typical chemical structure of ferroelectric LCEs and the electroclinic effect that induces the actuation. Reproduced with permission[121]. Copyright 2021, American Chemical Society; (C) schematic illustration of the core–shell 3D printing of LCE fibers composed of a liquid metal (LM) core surrounded by a LCE shell, and optical images of the electric actuation. Scale bar, 5 mm. Reproduced with permission[123]. Copyright 2021, Wiley-VCH; (D) LCE composites with LM droplets embedded in the LCE matrix and their mechanical responses. The bottom photographs demonstrate that the LCE/LM composites can be used as touch sensors. The LED turns on when the sensing composite responds to touch. Scale bars, 1 mm at the top panel and 1 cm at the bottom. Reproduced with permission[125]. Copyright 2019, National Academy of Sciences.

### Actuation induced by other stimuli

LCEs can deform in response to the chemical compositions (or called chemoresponsive), thus finding applications in chemical sensors (e.g., pH, humidity, metal ion sensors). The chemical actuation can be achieved by introducing breakable mesogenic units (or conformational-changed mesogenic units) or through the mechanism of anisotropic swelling. While LCEs are typically insensitive to chemical stimuli, the incorporation of reactive groups into the LCEs network allows the network to be broken down under special chemical signals (KOH solution[127,128] or enzymes[25,129]). For example, a LCE incorporated by the hydrogen-bonding carboxylic acid monomer experiences the neutralization of carboxylic acids, thus breaking down hydrogen bonds. Figure 7A gives a detailed example of an irreversible bond-breaking by the two-step reaction when the urease is tethered into the LCE network[25]. The LCE exhibited a contraction of up to 36%. Figure 7B shows the conformational change caused by the metal iron (Fe+) trapped in the 2,6-bisbenzimidazolylpyridine (Bip) mesogen[130]. When the LCE/Bip sample is immersed into the metal iron solution, the sample contracts along the length direction. Additionally, the LCE/Bip can respond to

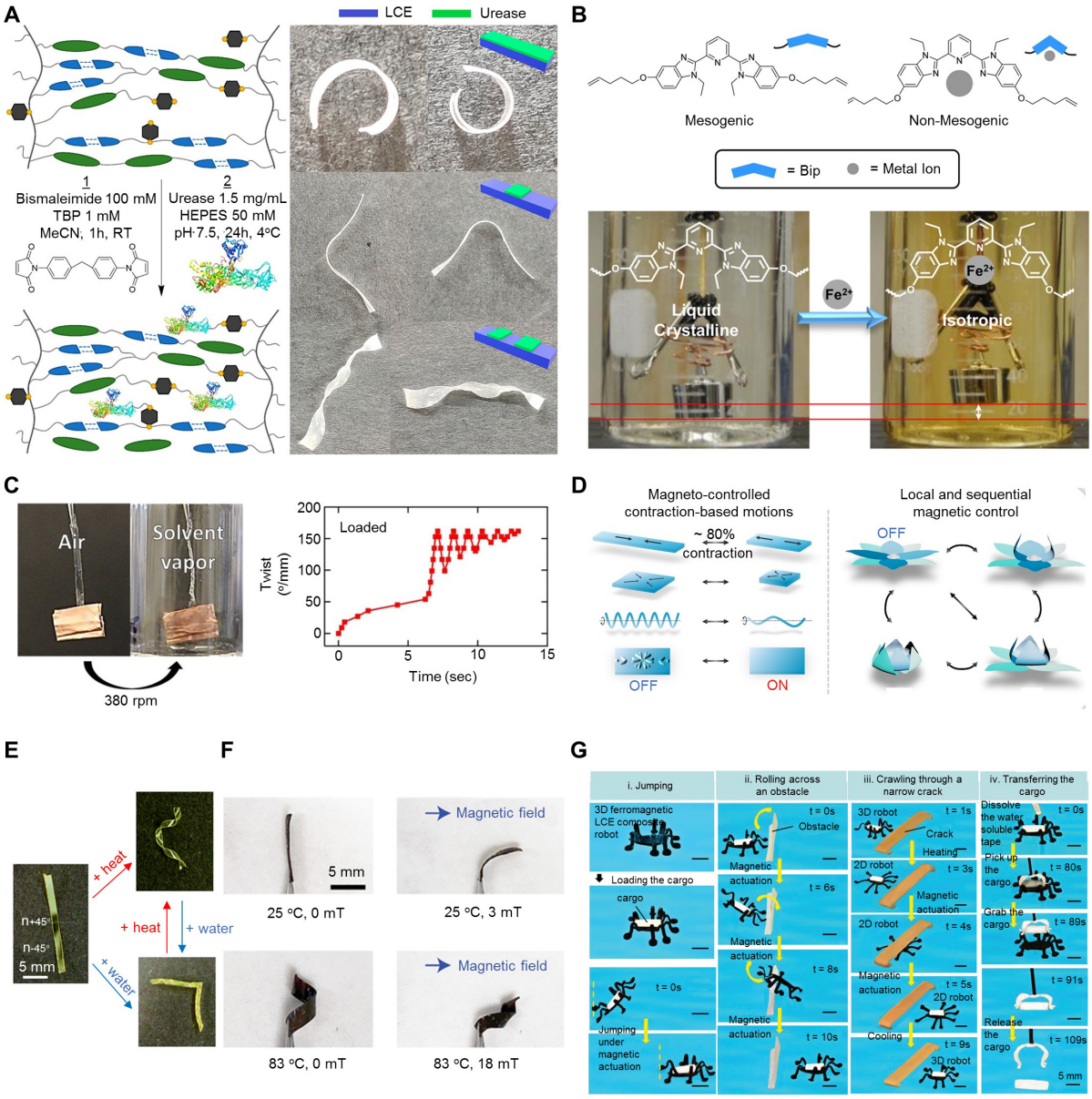


**Figure 7.** Actuation of LCEs by other stimuli. (A) Organic solvent stimulated actuation. The schematic illustration on the left shows the two-step chemical reaction of the urease with LCEs. The optical images on the right show the urease-stimulated deformation of LCE stripes, including bending and helix. Reproduced with permission[25]. Copyright 2021, American Chemical Society; (B) metal ion (Fe+) stimulated actuation. The schematic illustration shows that the mesogens/Bip changes from mesogenic phase to nonmesogenic phase upon binding the metal ion (Fe+). The photograph on the bottom shows that the LCE sample undergoes a macroscopic contraction after the actuation. Reproduced with permission[130]. Copyright 2021, American Chemical Society; (C) swelling-induced actuation. The left photograph shows an isotropic shape actuation triggered by immersing in the solvent vapor. The right figure shows a time-dependent twist during the swelling-induced actuation. Reproduced with permission[132]. Copyright 2017, Elsevier; (D) magnetothermal actuation. The schematic illustration shows the basic deformation mode and the controlling strategy for the LCEs responsive to the magnetic field. Reproduced with permission[43]; (E) deformation of a LCE stripe under the combined thermal and swelling actuation. Scale bar, 5 mm. Reproduced with permission. Copyright 2017, The Royal Society of Chemistry; (F) deformation of a LCE-based composite under the combined photothermal and magnetic actuation. Reproduced with permission[135]. Copyright 2021, Wiley-VCH GmbH; (G) a ferromagnetic LCE actuated by combined temperature and magnetic fields. The photograph shows a multi-function robot constructed by the ferromagnetic LCE. The robot can jump, roll, crawl, and carry loads. Scale bars, 5 mm. Reproduced with permission[44]. Copyright 2021, Wiley-VCH.

thermo- and photo-signals, thus enabling a complex actuation behavior by the combined stimuli. LCEs swell under different solvents, including water[128], KOH solution[131], and organic solvents[132]. Figure 7C shows that low molar mass LCEs actuate both axially and torsionally when immersed in organic solvents (tetrahydrofuran, acetone, dimethylformamide, and chloroform)[132].

Magnetic actuation of LCEs is also possible by incorporating magnetic nanoparticles. J. Zhang *et al.*[133] incorporated hard NdFeB magnetic microparticles into the LCEs, enabling an actuation strain of ~10% through magnetic control. The magnetically actuated LCEs could be controlled remotely in enclosed environments[43], holding promise for implanted applications inside the human body. However, adding magnetic particles to the LCEs could increase the stiffness of the LCEs and reduce their stretchability (e.g., from ~30% to 20%)[134]. Figure 7D provides an example where the $Fe_3O_4$ nanoparticles are dispersed into the polyurethane LCE to render magnetic responsiveness[43]. This LCE-based composite can realize a giant contraction strain (~80%) and offer a reprogrammable actuation capability (i.e., the actuation mode can easily be written and erased). The magnetic LCEs deform under relatively high magnetic flux density (~50Gs)[43], requiring complicated auxiliary and bulkier actuation/control equipment (e.g., alternating magnetic fields device in Ref.[43]). Besides, the magnetic flux density generates massive magnetic field-induced heating; thus, the energy efficiency for magnetic actuation is low.

The heterogeneous integration of different stimuli-responsive materials allows the actuation of LCE-based composite under multiple external fields. Figure 7E shows a thin stripe integrating two LCE layers with different alignment directions, which responds to different stimuli (temperature and humidity). This LCE composite deforms into a stable helical shape under an elevated temperature and further into another shape after immersion into the water. Figure 7F presents a bilayer film composed of LCE and magnetic responsive elastomers, which can achieve a complex dual-responsive shape morphing[135]. This bilayer composite was used in the demonstration of a legged mobile robot that can sense the environment temperature and move under the magnetic field. Figure 7G presents ferromagnetic LCE composites that deform in response to both thermal and magnetic fields[44]. Such composites can be exploited to design a "bug" robot capable of multimodal locomotion, e.g., jumping, rolling and crawling.

## APPLICATIONS OF LCES

### Soft robotics

LCE-based robots can achieve various types of locomotion modes, such as crawling[136-138], rolling[46,63], jumping[139], climbing[89,114], and swimming[113]. Figure 8A presents a free-standing wavy 3D ring that shows either a highly symmetric shape or a symmetry-broken twisted shape[140]. When placed on a hot surface or under remote infrared light, these rings can self-crawl along a pre-defined axis of symmetry via self-sustained flipping. Figure 8B shows a LCE-based rolling robot that can be reshaped into an origami polyhedral shape from the initial 2D planar configuration[46]. Upon heating, the rolling robot can be assembled into a pentagonal prism (perimeter ~15 mm) and then self-roll with a speed of 0.13 cm/s. Figure 8C shows a light-driven soft jumping robot based on a double-folded LCE actuator with a three-leaf folding structure[139]. By changing the size and crease angle of the double-folded LCE actuator, the height, distance, and direction of the jumping motion can be adjusted. It is noteworthy that this robot can achieve remarkable jumping height (87 times body length), jumping distance (65 times body length), and maximum take-off velocity (930 times body length/s). Figure 8D presents voltage-driven climbing robots, mainly composed of the LCE with integrated conductive wires[47]. The deformable electro-adhesive footpad and smart joint allow the climbing of the robot on diverse curvy surfaces and switching between two different surfaces. Figure 8E illustrates a robot consisting of the LCEs with embedded magnetic microparticles[133]. This reconfigurable robot can simultaneously swim in a viscous media and walk in the air.

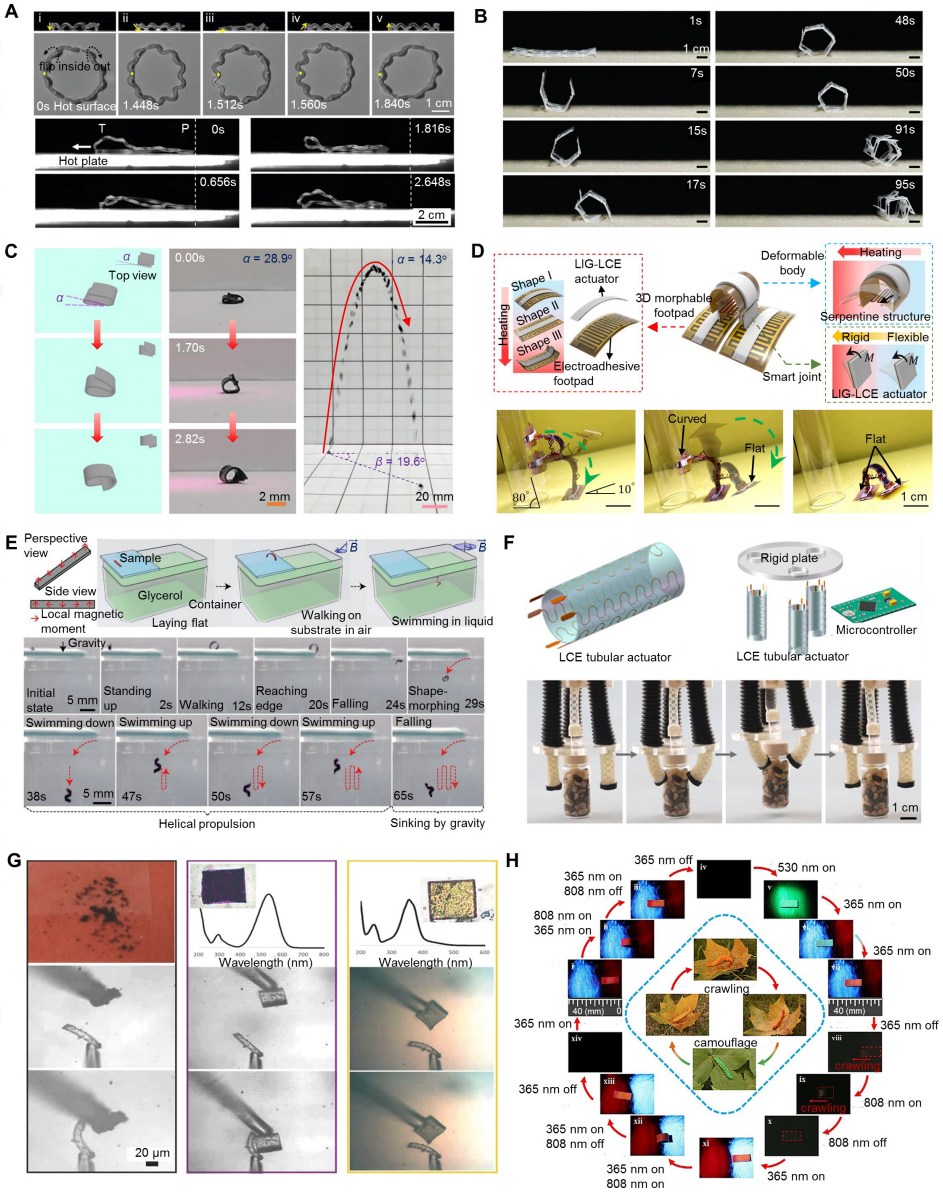


**Figure 8.** Application in soft robotics. (A) Self-crawling robot. The robot with a twisted ring shape offers a tunable moving speed at different temperatures. Scale bar, 2 cm. Reproduced with permission[140]. Copyright 2022, Wiley-VCH GmbH; (B) rolling robot. The robot can realize the self-folding (from 2D shape to 3D cylindrical shape) and self-rolling under thermal actuation. Scale bars, 1 cm. Reproduced with permission[46]. Copyright 2019, American Association for the Advancement of Science; (C) jumping robot. The robot has a double-folded ribbon shape, exhibiting an excellent jumping performance under the optical actuation. Scale bars, 2 mm at the middle panel and 20 mm at the right. Reproduced with permission[139]. Copyright 2023, Wiley-VCH; (D) climbing robot. The robot can climb on various curvy surfaces, and switch between two different surfaces, by harnessing the electrothermal actuation. Scale bars, 1 cm. Reproduced with permission[47]. Copyright 2022, National Academy of Science; (E) swimming robot. The geometrically reconfigurable robot (arc-shaped in the air and helix-shaped in the viscous liquid) can walk, jump, and swim in response to remote thermal/magnetic fields. Scale bars, 5 mm. Reproduced with permission[133]. Copyright 2021, Wiley-VCH; (F) macroscopic gripper. The schematic illustration shows an electrically controlled gripper consisting of three tubular LCE actuators, a microcontroller, and a fixture. The optical images on the bottom show that the gripper can realize grabbing, holding and releasing. Scale bar, 1 cm. Reproduced with permission[45]. Copyright 2019, American Association for the Advancement of Science; (G) microgripper. The photograph shows that the microgripper autonomously grabs certain materials. Scale bar, 20 μm. Reproduced with permission[141]. Copyright 2017, WILEY-VCH; (H) camouflage robot. The schematic illustration shows a biomimetic robot that can crawl and discolor in response to light with different wavelengths. Reproduced with permission[142]. Copyright 2021, Wiley-VCH.

Owing to the relatively large actuation stress, high actuation strain, and versatile actuation modes, LCEs can be used as grippers at different length scales[44,88,143]. Figure 8F presents a LCE-based tubular actuator with multiple actuation modes powered by electricity[45]. The gripper, capable of grasping and releasing 50 g vials, is composed of LCE actuators, a fixing plate, and a microcontroller. The gripper can be fabricated in micro-scale size via various methods (e.g., soft lithography, 3D printing, embossing, et. at.)[141,144,145]. Figure 8G shows a photothermally actuated microgripper (20 × 200 × 20 $\mu m^3$) fabricated by soft lithography[141]. This microgripper recognizes objects by the response to certain spectra from the resonant laser lines of the target material. The microgripper only grabs the recognized material.

Specially prepared LCEs can change their shape and colors spontaneously, which can be used to develop the LCE-based camouflage robot[102,142,146-149]. Figure 8H shows an example[142] based on the LCE that incorporates tetraphenylethene and spiropyran moieties. The resulting robot resembles a caterpillar and can walk (by shape-morphing) and camouflage (by discoloration) in response to light with different wavelengths.

### Temperature/Strain sensors

The nematic LCEs could change transmittance following the phase transition induced by mechanical or thermal loadings, which have been exploited to develop temperature or strain sensors. LCEs are opaque at the nematic polydomain state and become transparent when heated into the isotropic phase. Based on this optical behavior, a temperature sensor with integrated a light intensity sensor, light-emitting diodes (LEDs), and a buzzer indicator was developed, as shown in Figure 9A[150]. When the environment temperature changes, the light intensity across the LCE film changes and is measured by the light intensity sensor. Based on the magnitude of the temperature, the LEDs display different colors (red, yellow, and green). When the temperature reaches a dangerous level, the LEDs turn red and the buzzer indicator sounds to inform the users. Based on the transmittance changes of LCEs caused by thermal and mechanical loadings, a strain sensor consisting of a LCE cantilever actuator and an infrared radiation (IR) LED [Figure 9B] was prepared[14]. The sensor possesses two modes of bending deformations, including thermally induced and nonthermally induced modes. In the thermal bending mode, the beam becomes more transparent at a higher temperature, resulting in a stronger optical signal, and this optical signal becomes stronger with the increase of the bending strain. In the nonthermal bending mode, the LCE beam is almost opaque at the nematic state, yielding a weaker signal than the case of the thermal bending mode. According to the measured optical signals and temperature history, the bending deformation can then be determined. In Figure 9C, Wei *et al.*[151] reported a photoresponsive device composed of LCE, graphene-doped polydimethylsiloxane (PDMS), and polyvinylidene fluoride (PVDF) layers, which can effectively convert photothermal and mechanical energies into electricity. It is noteworthy that the device could be powered by near-infrared radiation (NIR). Because of the temperature fluctuation induced by NIR light, the bending angles are time-varying, which can be measured for temperature sensing. Figure 9D presents LCE-LM coaxial fibers consisting of LCE fibers with a hollow structure and LM in the core[152]. Through Joule heating, the inner LM can generate heat to actuate the outer LCE shell. When the LCE–LM fiber is uniaxially stretched, the resistance of the inner LM changes, thereby allowing us to determine the extension of the fibers or the mass of loading from the resistance change of the inner LM.

Unlike the nematic LCEs, cholesteric LCEs usually exhibit color changes under mechanical or thermal loadings, and this feature can be used for strain/temperature sensing. For example, a strain sensor was designed based on a stretchable and highly uniform cholesteric LCE film [Figure 9E][48]. When the film is under a bending strain with zero Gaussian curvature, the film turns blue gradually. Differently, when the film is under a bending strain with nonzero Gaussian curvature, the two parts separated by a gap show different colors (e.g., red and blue). By monitoring the color changes, the local bending strain could be determined, and the deformation modes with different curvatures could be distinguished. Additionally, the

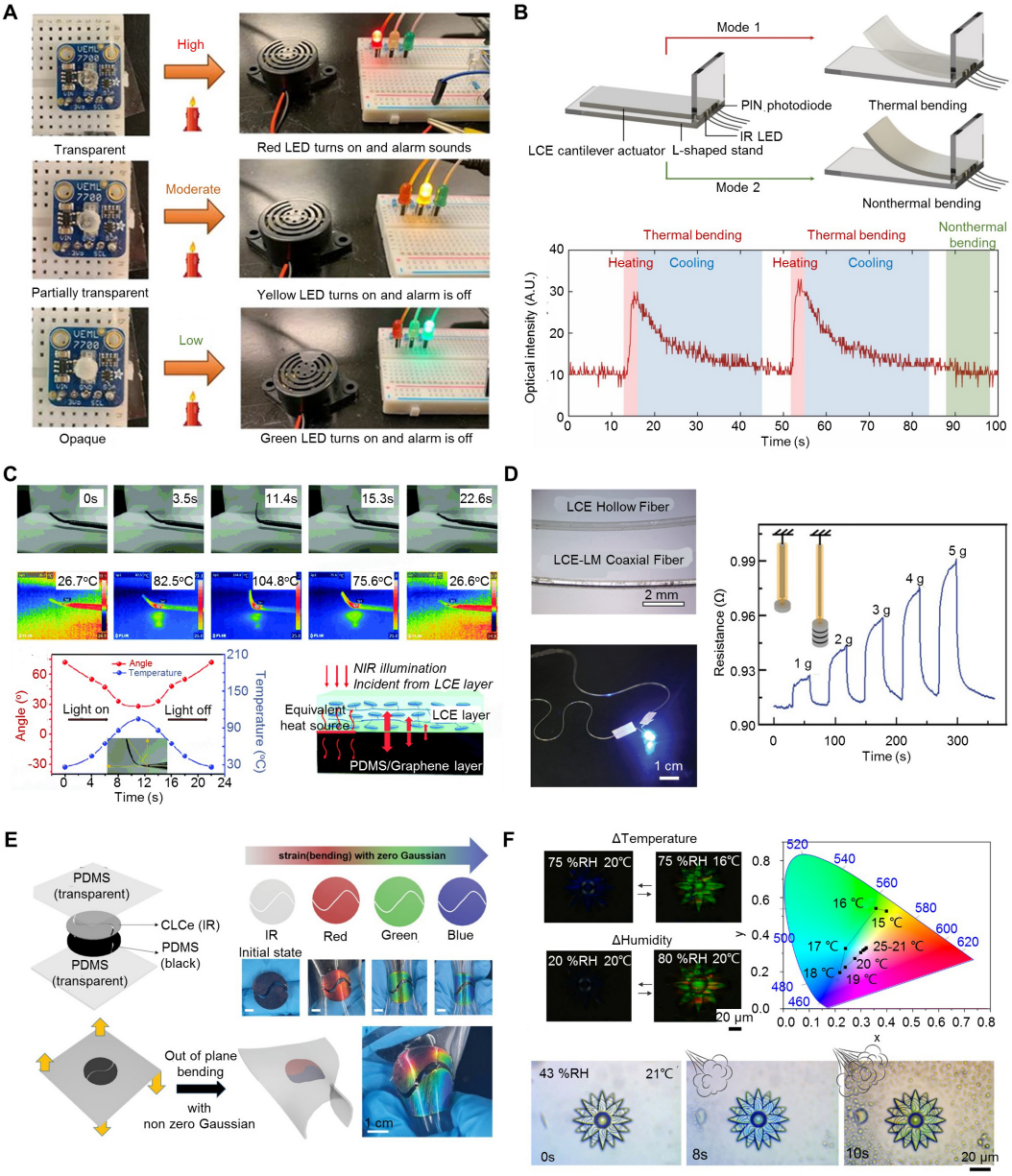


**Figure 9.** Application in temperature and strain sensors. (A) Temperature sensor based on the transmittance change of the LCE film due to temperature change. When the temperature is above a safety threshold, the red LED turns on and an alarm sounds to alert the users. Reproduced with permission[150]. Copyright 2022, American Chemical Society; (B) self-sensing cantilever actuator with integrated miniature optoelectronic components. Thermal and nonthermal bending modes could be experienced, and the real-time optical intensity is measured for the monitoring of the bending deformation. Reproduced with permission[14]. Copyright 2021, American Association for the Advancement of Science; (C) NIR light and temperature sensor based on the photothermal pyroelectric property. Reproduced with permission[151]. Copyright 2018, The Royal Society of Chemistry; (D) LM-LCE coaxial fibers, which could sense the fiber stretching by measuring the voltage or resistance change of the inner LM. Scale bars, 2 mm at the top panel and 1 cm at the bottom. Reproduced with permission[152]. Copyright 2021, Wiley-VCH GmbH; (E) strain sensor based on highly stretchable and highly uniform main-chain cholesteric LCE film, which could change color at different strain levels. The film is continuously blue-shifted and homogenous under a bending strain with zero Gaussian curvature. When the film is bent with nonzero Gaussian curvature, the two parts separated by a gap show different colors (e.g., red and blue). Scale bar, 1 cm. Reproduced with permission[48]. Copyright 2022, Wiley-VCH GmbH; (F) environmental temperature and humidity sensor, showing a color change from transparent to blue to green when the humidity increases or the temperature decreases. Scale bar, 20 μm. Reproduced with permission[49]. Copyright 2020, American Chemical Society.

color change of the cholesteric LCE could also be achieved by the volume expansion of the helix director induced by the temperature or humidity change[49]. A photonic flower-like sensor based on the cholesteric LCE was developed, which shifted the color from colorless to light blue, and then to bright green, with decreasing temperature or increasing humidity [Figure 9F][49].

### Biomedical devices

In addition to excellent actuation and sensing capabilities, specially designed LCEs also offer good biocompatibility, thereby holding potential for biomedical applications. For example, Figure 10A shows 3D biodegradable and highly regular foamlike cell scaffolds fabricated based on biocompatible porous side-chain LCEs[51]. The SEM images show that the cell scaffolds have similar architectures of vascular networks in tissue. Fluorescence confocal microscopy images of myoblast cells proved the biocompatibility of the LCEs. Such scaffolds show four times higher cell proliferation capability compared to conventional porous template films[51]. Figure 10B illustrates an artificial intervertebral disc based on the monodomain LCE around the exterior and polydomain LCE in the center[153]. Such intervertebral disc possesses similar mechanical properties (e.g., modulus and anisotropy) to an actual one, which could be used as an implantable device for tissue growth.

Aside from biocompatibility, LCEs also possess muscle-like actuation capabilities. By optimizing the actuation performances, Wu *et al.*[52] developed a breathable, shrinkable, hemostatic patch, which consists of a LCE metamaterial layer with a low actuation temperature (~46 °C) and a waterproof dressing layer to offer combined physical and chemical treatments [Figure 10C]. Such a patch could provide a suitable biaxial contraction (~10 kPa; close to the tensile of the *in vivo* skin) and biaxial actuation strain (~23%) when heated from 25 °C to 46 °C. By this noninvasive means, skin regeneration can be accelerated while avoiding scar and keloid generation. Figure 10D illustrates an implanted LCE-based device with IR-absorbing carbon black (CB) particles[50]. The LCE-CB composites can change shape in response to temperature increase induced by the transcutaneous IR light. This device could be implanted as an artificial cuff or sphincter around the bladder neck to control the urine flow by the contraction forces induced by IR light, with the potential to treat stress urinary incontinence.

### Other applications

Excluding the above promising applications, the LCEs could also be used for energy absorption, flexible display, liquid controlling, and smart textiles. By harnessing the soft elasticity of the LCEs, Traugutt *et al.*[12] fabricated various 3D porous LCE lattices for efficient energy absorption [Figure 11A]. Compared with the elastomer (TangoBlack) lattice, the LCE lattice offers 12 times higher rate-dependency and 27 times higher strain energy density. Based on the optomechanical responses of cholesteric LCEs, a highly stretchable cholesteric LCE film was fabricated by Hussain *et al.* [Figure 11B][154]. When the film is stretched, the film could reflect both left- and right-handed circular polarized lights with blue-shifted color. By controlling the applied strain, polarized light, or temperature, the film could display or vanish the patterns, which could be used in flexible displays and data encryption. In Figure 11C, Q. Liu *et al.* fabricated tubular LCE microactuators whose shapes could be changed by the gradient of light[53]. As a result, the liquid in the tube could be driven into the narrow end. Using this technique, the velocity and direction of liquids could be well remotely controlled by light over a long distance. In Figure 11D, the LCE fibers with reversible thermal actuation were knit, sewn, and woven to fabricate smart textiles[54]. Together with woven conductive fibers, the LCE fibers could be sewn into a shirt, which could create proper pores to reduce users' body temperature on a hot day.

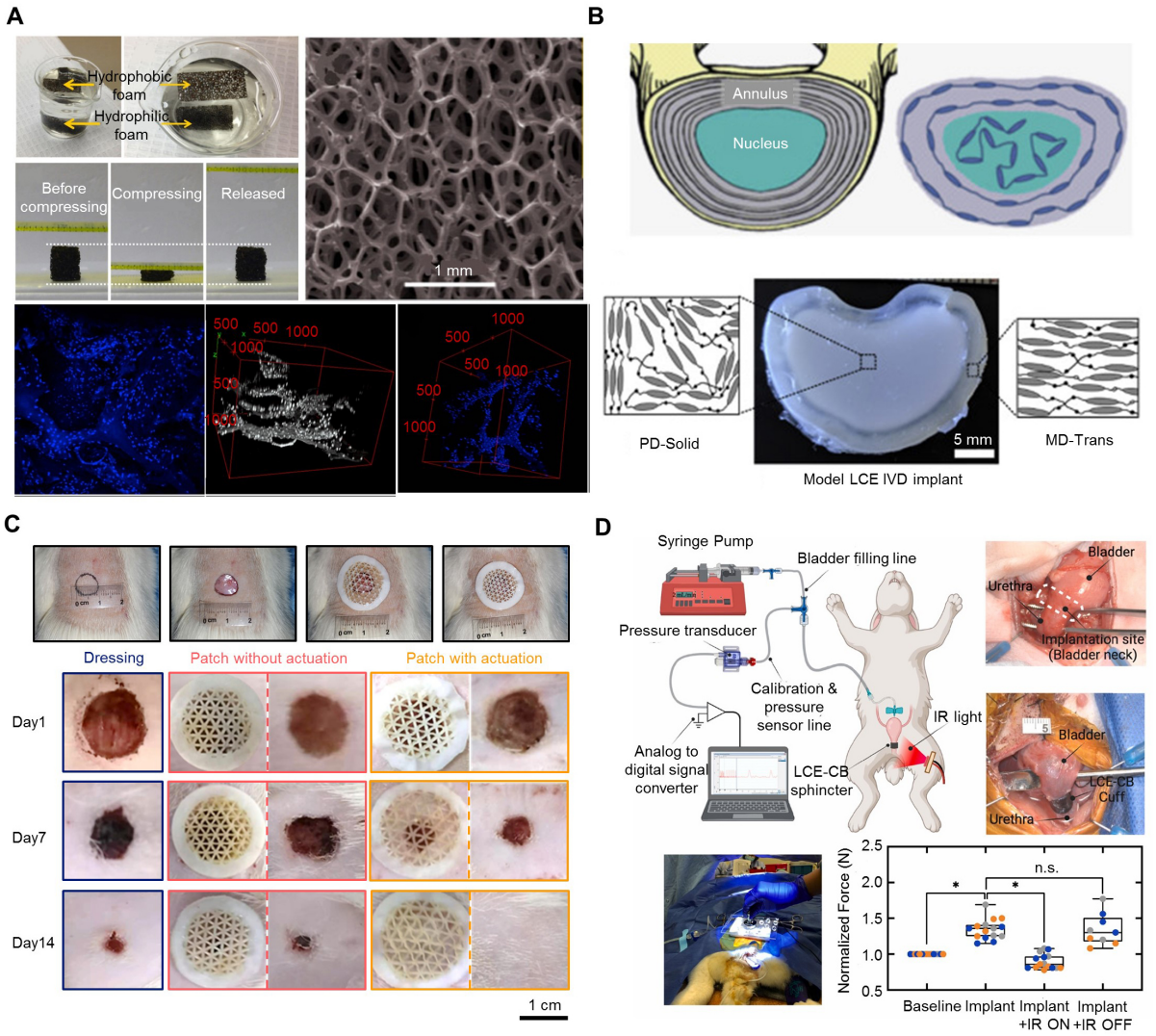


**Figure 10.** Application in biomedical devices. (A) 3D biodegradable and highly regular foamlike cell scaffolds based on biocompatible side-chain liquid crystal elastomers. Scale bars, 1 mm. Reproduced with permission[51]. Copyright 2016, American Chemical Society; (B) an artificial intervertebral disc for tissue growth. Scale bar, 5 mm. Reproduced with permission[153]. Copyright 2020, Elsevier; (C) breathable, shrinkable, hemostatic LCE patch for accelerating skin regeneration in a rat model. Scale bar, 1 cm. Reproduced with permission[52]. Copyright 2021, Wiley VCH; (D) an implanted LCE-based device as an artificial cuff or sphincter around the bladder neck, which can control the urine flow by contraction force. Reproduced with permission[50]. Copyright 2022, Elsevier.

## CONCLUSION AND OUTLOOK

We summarize the recent progress in the developments of LCEs, covering their fabrication, designs, actuation mechanisms and applications. Chemical synthesis methods are revisited initially, including two-stage and one-pot reactions. Among the methods based on the two-stage reaction, the 3D/4D printing methods are very promising because of their powerful manufacturing capabilities in achieving high levels of geometric complexity. Based on the one-pot reaction, the surface-enforced method can be adopted for programming the alignment in a thin film by combining it with advanced microfabrication methods. Then, the actuation mechanisms are discussed, and a variety of actuation responses are elaborated, under different types of stimuli, such as thermal, optical, electric, magnetic, and chemical stimuli. Strikingly, the LCE-based actuators can realize remote control under optical, thermal, or magnetic actuation. Usually, the magnetic or chemical actuation can be combined with other mechanisms to develop multifunctional actuators

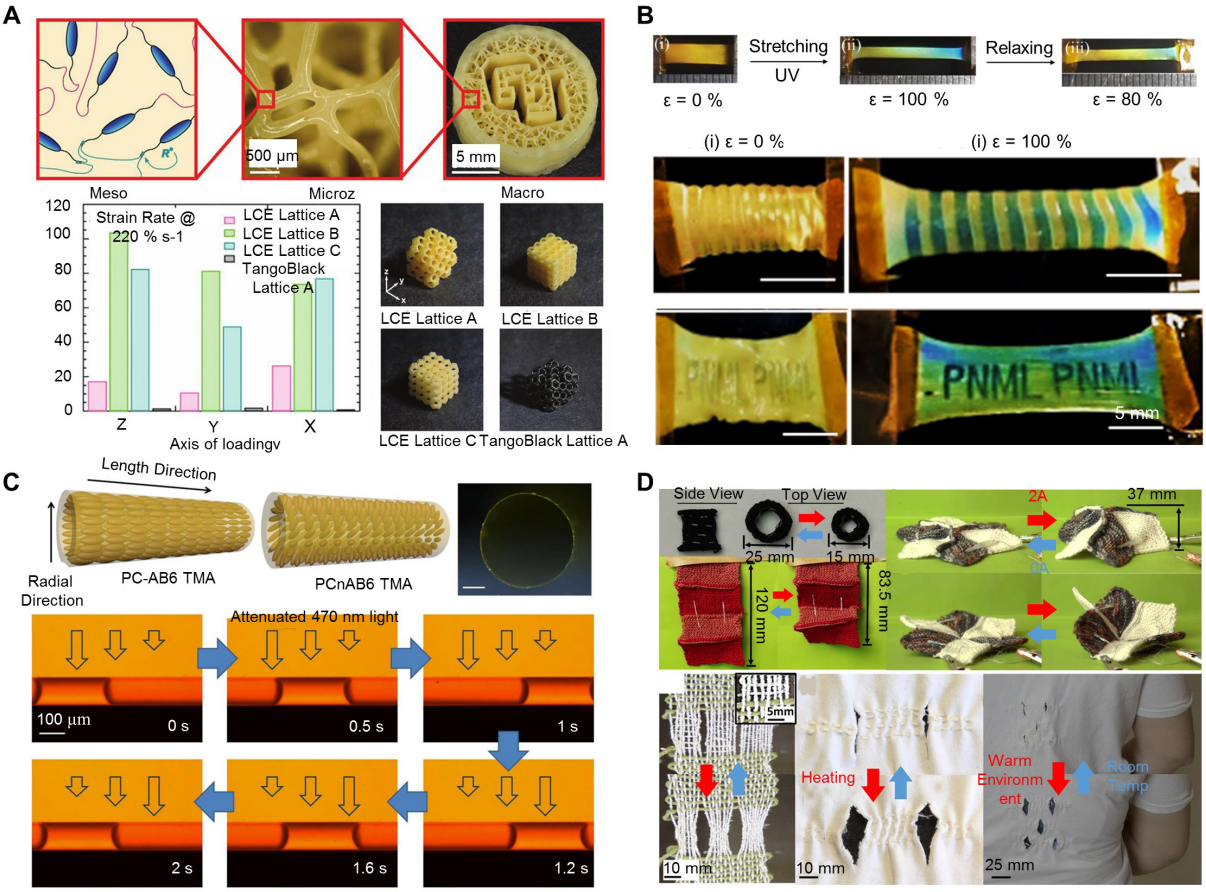


**Figure 11.** Other applications of LCEs. (A) LCE-based dissipative structures with high energy-absorbing capabilities, fabricated by 3D printing. Scale bars, 200 μm and 5 mm in the middle and right panels. Reproduced with permission[12]. Copyright 2020, WILEY-VCH; (B) highly stretchable mechanochromic photonic cholesteric LCE film for use as flexible displays. Scale bars, 5 mm. Reproduced with permission[154]. Copyright 2021, American Chemical Society; (C) tubular LCE microactuators, which could exert photocontrol of a wide diversity of liquids over a long distance with controllable velocity and direction. Scale bar, 100 μm. Reproduced with permission[53]. Copyright 2019, Wiley-VCH; (D) stimulus-responsive LCE fiber-based smart textiles to create on-demand pores to reduce the wearer's body temperature during exercise. Scale bars, 10 mm in the left panel and 25 mm in the right. Reproduced with permission[54]. Copyright 2019, American Chemical Society.

responsive to multiple different stimuli. Finally, the emerging applications of the LCEs are presented, including soft robotics, temperature/strain sensors, and novel biomedical devices, among others.

Despite the extensive research progress, many scientific and technological challenges still exist. The fabrication and alignment techniques limit the thickness and pattern precision of LCEs, which could not well meet the requirement of the micro-actuators with feature sizes below 10 μm. The limitation of the minimum size of the LCE-based actuators fabricated by the digital light processing 3D printing reported is ~50 μm[14,30]. With the development of advanced fabrication techniques (e.g., lithography, inkjet printing, microfluidics, and electrospinning), the miniaturization of the LCE actuators and relevant devices may be realized.

The actuation performances for LCEs and their composites require further improvements. The actuation strain and stress are mainly influenced by the fabrication method and chemical compositions. For example, the actuation stress can be adjusted by the temperature difference between the initial temperature and the

nematic-isotropic transition temperature, and a smaller temperature difference provides a smaller actuation stress of LCEs, limiting their applications in a mild environment like human body temperature (~37 °C). Additionally, the actuation speed requires further improvements to be suited for applications that require fast responses. The heating/cooling time of the thermally or optically driven LCEs is quite long[117] because of the low efficiency of heat transferring. The response time can be further improved by reducing the LCE dimensions because smaller and thinner LCEs offer faster actuation deformations. Furthermore, to accelerate the cooling time, some available solutions were provided in our revised manuscript, such as embedding LM droplets, doping CB nanoparticles, and integrating microfluidic channels to pump cold fluids[47].

LCE-based 3D architected materials represent an underexplored area due to the challenges in the fabrication. Most existing LCE-based devices are initially strips or films before the alignment. It is clear that 3D architected actuators can offer more deforming modes and versatile shape-morphing capabilities than planar actuators. However, it remains challenging to fabricate highly curvy 3D LCE architectures, such as the chiral[155] or helical[156] networks, or other 3D-shaped structures[157].

## DECLARATIONS

### Acknowledgments

Y.Z. acknowledges the support from the National Natural Science Foundation of China (grant Nos. 12225206, 12050004, and 11921002), the Tsinghua National Laboratory for Information Science and Technology, the Henry Fok Education Foundation (grant No. 171003), a grant from the Institute for Guo Qiang, Tsinghua University (grant No. 2021GQG1009), and the XPLORER PRIZE from the Tencent Foundation.

### Authors' contributions

Conceptualization, investigation, wrote the original draft: Xiao Y, Wu J
Reviewed and revised the manuscript: Zhang Y
Supervision, project administration, funding acquisition: Zhang Y

### Availability of data and materials

Not applicable.

### Financial support and sponsorship

Y.Z. acknowledges the support from the National Natural Science Foundation of China (grant Nos. 12225206, 12050004, and 11921002), the Tsinghua National Laboratory for Information Science and Technology, the Henry Fok Education Foundation (grant No. 171003), a grant from the Institute for Guo Qiang, Tsinghua University (grant No. 2021GQG1009), and the XPLORER PRIZE from the Tencent Foundation.

### Conflicts of interest

All authors declared that there are no conflicts of interest.

### Ethical approval and consent to participate

Not applicable.

### Consent for publication

Not applicable.

## REFERENCES

1. Gao Y, Sun D, Chen J, et al. Photoelastic Organogel with Multiple Stimuli Responses. *Small* 2022;18:e2204140. DOI
2. Lu T, Ma C, Wang T. Mechanics of dielectric elastomer structures: a review. *Extreme Mech Lett* 2020;38:100752. DOI
3. Gao Y, Chen J, Han X, et al. A universal strategy for tough adhesion of wet soft material. *Adv Funct Mater* 2020;30:2003207. DOI
4. Herbert KM, Fowler HE, Mccracken JM, Schlafmann KR, Koch JA, White TJ. Synthesis and alignment of liquid crystalline elastomers. *Nat Rev Mater* 2022;7:23-38. DOI
5. Kim DH, Lu N, Ma R, et al. Epidermal electronics. *Science* 2011;333:838-43. DOI
6. Choi S, Lee H, Ghaffari R, Hyeon T, Kim DH. Recent advances in flexible and stretchable bio-electronic devices integrated with nanomaterials. *Adv Mater* 2016;28:4203-18. DOI
7. Lu N, Kim D. Flexible and stretchable electronics paving the way for soft robotics. *Soft Robot* 2014;1:53-62. DOI
8. Guo X, Liu L, Zhou B, Liu Y, Leng J. Influence of strain rates on the mechanical behaviors of shape memory polymer. *Smart Mater Struct* 2015;24:095009. DOI
9. Guo X, Ni X, Li J, et al. Designing mechanical metamaterials with kirigami-inspired, hierarchical constructions for giant positive and negative thermal expansion. *Adv Mater* 2021;33:e2004919. DOI
10. Zhang Y, Zhang N, Hingorani H, et al. Fast-response, stiffness-tunable soft actuator by hybrid multimaterial 3D printing. *Adv Funct Mater* 2019;29:1806698. DOI
11. Ge Q, Chen Z, Cheng J, et al. 3D printing of highly stretchable hydrogel with diverse UV curable polymers. *Sci Adv* 2021;7:eaba4261. DOI PubMed PMC
12. Traugutt NA, Mistry D, Luo C, Yu K, Ge Q, Yakacki CM. Liquid-crystal-elastomer-based dissipative structures by digital light processing 3D printing. *Adv Mater* 2020;32:e2000797. DOI
13. Zhang X, Yao L, Yan H, et al. Optical wavelength selective actuation of dye doped liquid crystalline elastomers by quasi-daylight. *Soft Matter* 2022;18:9181-96. DOI
14. Li S, Bai H, Liu Z, et al. Digital light processing of liquid crystal elastomers for self-sensing artificial muscles. *Sci Adv* 2021:7. DOI
15. Liang X, Li D. A Programmable liquid crystal elastomer metamaterials with soft elasticity. *Front Robot AI* 2022;9:849516. DOI PubMed PMC
16. Zhang Z, Huo Y. Programmable mechanical energy absorption and dissipation of liquid crystal elastomers: modeling and simulations. *Adv Eng Mater* 2022;24:2100590. DOI
17. White TJ, Broer DJ. Programmable and adaptive mechanics with liquid crystal polymer networks and elastomers. *Nat Mater* 2015;14:1087-98. DOI PubMed
18. Barnes M, Verduzco R. Direct shape programming of liquid crystal elastomers. *Soft Matter* 2019;15:870-9. DOI PubMed
19. Fang M, Liu T, Xu Y, et al. Ultrafast digital fabrication of designable architectured liquid crystalline elastomer. *Adv Mater* 2021;33:e2105597. DOI
20. Finkelmann H, Greve A, Warner M. The elastic anisotropy of nematic elastomers DOI
21. Lehmann W, Skupin H, Tolksdorf C, et al. Giant lateral electrostriction in ferroelectric liquid-crystalline elastomers. *Nature* 2001;410:447-50. DOI
22. Buguin A, Li MH, Silberzan P, Ladoux B, Keller P. Micro-actuators: when artificial muscles made of nematic liquid crystal elastomers meet soft lithography. *J Am Chem Soc* 2006;128:1088-9. DOI PubMed
23. Wang Z, He Q, Wang Y, Cai S. Programmable actuation of liquid crystal elastomers via “living” exchange reaction. *Soft Matter* 2019;15:2811-6. DOI
24. Guin T, Hinton HE, Burgeson E, et al. Tunable electromechanical liquid crystal elastomer actuators. *Adv Intell Syst* 2020;2:2000022. DOI
25. Abadia A, Herbert KM, Matavulj VM, White TJ, Schwartz DK, Kaar JL. Chemically triggered changes in mechanical properties of responsive liquid crystal polymer networks with immobilized urease. *J Am Chem Soc* 2021;143:16740-9. DOI PubMed
26. Saed MO, Elmadih W, Terentjev A, Chronopoulos D, Williamson D, Terentjev EM. Impact damping and vibration attenuation in nematic liquid crystal elastomers. *Nat Commun* 2021;12:6676. DOI PubMed PMC
27. Skačej G, Zannoni C. Main-chain swollen liquid crystal elastomers: a molecular simulation study. *Soft Matter* 2011;7:9983. DOI
28. Wang Z, Guo Y, Cai S, Yang J. Three-dimensional printing of liquid crystal elastomers and their applications. *ACS Appl Polym Mater* 2022;4:3153-68. DOI
29. Krause S, Dersch R, Wendorff JH, Finkelmann H. Photocrosslinkable liquid crystal main-chain polymers: thin films and electrospinning. *Macromol Rapid Commun* 2007;28:2062-8. DOI
30. Zhao J, Zhang L, Hu J. Varied alignment methods and versatile actuations for liquid crystal elastomers: a review. *Adv Intell Syst* 2022;4:2100065. DOI
31. Zhu C, Lu Y, Jiang L, Yu Y. Liquid crystal soft actuators and robots toward mixed reality. *Adv Funct Mater* 2021;31:2009835. DOI
32. Ohm C, Brehmer M, Zentel R. Liquid crystalline elastomers as actuators and sensors. *Adv Mater* 2010;22:3366-87. DOI PubMed
33. Ambulo CP, Tasmim S, Wang S, Abdelrahman MK, Zimmern PE, Ware TH. Processing advances in liquid crystal elastomers

provide a path to biomedical applications. *J Appl Phys* 2020;128:140901. DOI PubMed PMC

34. Pang W, Cheng X, Zhao H, et al. Electro-mechanically controlled assembly of reconfigurable 3D mesostructures and electronic devices based on dielectric elastomer platforms. *Natl Sci Rev* 2020;7:342-54. DOI
35. Visschers FLL, Hendrikx M, Zhan Y, Liu D. Liquid crystal polymers with motile surfaces. *Soft Matter* 2018;14:4898-912. DOI PubMed
36. Pang X, Lv JA, Zhu C, Qin L, Yu Y. Photodeformable azobenzene-containing liquid crystal polymers and soft actuators. *Adv Mater* 2019;31:e1904224. DOI PubMed
37. Wang Z, Cai S. Recent progress in dynamic covalent chemistries for liquid crystal elastomers. *J Mater Chem B* 2020;8:6610-23. DOI PubMed
38. Shaha RK, Torbati AH, Frick CP. Body-temperature s hape-shifting liquid crystal elastomers. *J Appl Polym Sci* 2021;138:50136. DOI
39. Traugutt NA, Volpe RH, Bollinger MS, et al. Liquid-crystal order during synthesis affects main-chain liquid-crystal elastomer behavior. *Soft Matter* 2017;13:7013-25. DOI
40. Kuenstler AS, Kim H, Hayward RC. Liquid crystal elastomer waveguide actuators. *Adv Mater* 2019;31:e1901216. DOI PubMed
41. Ahn S, Ware TH, Lee KM, Tondiglia VP, White TJ. Photoinduced topographical feature development in blueprinted azobenzene-functionalized liquid crystalline elastomers. *Adv Funct Mater* 2016;26:5819-26. DOI
42. Wang C, Sim K, Chen J, et al. Soft ultrathin electronics innervated adaptive fully soft robots. *Adv Mater* 2018;30:e1706695. DOI
43. Wu Y, Zhang S, Yang Y, Li Z, Wei Y, Ji Y. Locally controllable magnetic soft actuators with reprogrammable contraction-derived motions. *Sci Adv* 2022;8:eabo6021. DOI PubMed PMC
44. Li Y, Yu H, Yu K, Guo X, Wang X. Reconfigurable three-dimensional mesotructures of spatially programmed liquid crystal elastomers and their ferromagnetic composites. *Adv Funct Mater* 2021;31:2100338. DOI
45. He Q, Wang Z, Wang Y, Minori A, Tolley MT, Cai S. Electrically controlled liquid crystal elastomer-based soft tubular actuator with multimodal actuation. *Sci Adv* 2019;5:eaax5746. DOI PubMed PMC
46. 46. Kotikian A, McMahan C, Davidson EC et al. Untethered soft robotic matter with passive control of shape morphing and propulsion. *Sci Robot* 2019;4:eaax7044. DOI
47. Pang W, Xu S, Wu J, et al. A soft microrobot with highly deformable 3D actuators for climbing and transitioning complex surfaces. *Proc Natl Acad Sci USA* 2022;119:e2215028119. DOI PubMed PMC
48. Han WC, Lee YJ, Kim SU, Lee HJ, Kim YS, Kim DS. Versatile mechanochromic sensor based on highly stretchable chiral liquid crystalline elastomer. *Small* 2023;19:e2206299. DOI PubMed
49. Pozo M, Delaney C, Bastiaansen CWM, Diamond D, Schenning APHJ, Florea L. Direct laser writing of four-dimensional structural color microactuators using a photonic photoresist. *ACS Nano* 2020;14:9832-9. DOI PubMed PMC
50. Tasmim S, Yousuf Z, Rahman FS, et al. Liquid crystal elastomer based dynamic device for urethral support: potential treatment for stress urinary incontinence. *Biomaterials* 2023;292:121912. DOI PubMed PMC
51. Gao Y, Mori T, Manning S, et al. Biocompatible 3D liquid crystal elastomer cell scaffolds and foams with primary and secondary porous architecture. *ACS Macro Lett* 2016;5:4-9. DOI
52. Wu J, Yao S, Zhang H, et al. Liquid crystal elastomer metamaterials with giant biaxial thermal shrinkage for enhancing skin regeneration. *Adv Mater* 2021;33:e2106175. DOI
53. Liu Q, Liu Y, Lv J, Chen E, Yu Y. Photocontrolled liquid transportation in microtubes by manipulating mesogen orientations in liquid crystal polymers. *Adv Intell Syst* 2019;1:1900060. DOI
54. Roach DJ, Yuan C, Kuang X, et al. Long liquid crystal elastomer fibers with large reversible actuation strains for smart textiles and artificial muscles. *ACS Appl Mater Interf* 2019;11:19514-21. DOI
55. Finkelmann H, Kock H, Rehage G. Investigations on liquid crystalline polysiloxanes. *Makromol Chem Rapid Commun* 1981;2:317-22. DOI
56. Yakacki CM, Saed M, Nair DP, Gong T, Reed SM, Bowman CN. Tailorable and programmable liquid-crystalline elastomers using a two-stage thiol–acrylate reaction. *RSC Adv* 2015;5:18997-9001. DOI
57. Kotikian A, Truby RL, Boley JW, White TJ, Lewis JA. 3D printing of liquid crystal elastomeric actuators with spatially programed nematic order. *Adv Mater* 2018;30:1706164. DOI PubMed
58. Enz E, Baumeister U, Lagerwall J. Coaxial electrospinning of liquid crystal-containing poly(vinylpyrrolidone) microfibres. *Beilstein J Org Chem* 2009;5:58. DOI PubMed PMC
59. Ohm C, Morys M, Forst FR, et al. Preparation of actuating fibres of oriented main-chain liquid crystalline elastomers by a wetspinning process. *Soft Matter* 2011;7:3730. DOI
60. Ohm C, Serra C, Zentel R. A continuous flow synthesis of micrometer-sized actuators from liquid crystalline elastomers. *Adv Mater* 2009;21:4859-62. DOI PubMed
61. Zeng H, Wani OM, Wasylczyk P, Kaczmarek R, Priimagi A. Self-regulating iris based on light-actuated liquid crystal elastomer. *Adv Mater* 2017;29:1701814. DOI PubMed
62. Aharoni H, Xia Y, Zhang X, Kamien RD, Yang S. Universal inverse design of surfaces with thin nematic elastomer sheets. *Proc Natl Acad Sci USA* 2018;115:7206-11. DOI PubMed PMC
63. Wang Z, Li K, He Q, Cai S. A light-powered ultralight tensegrity robot with high deformability and load capacity. *Adv Mater* 2019;31:e1806849. DOI

64. Shahsavan H, Aghakhani A, Zeng H, et al. Bioinspired underwater locomotion of light-driven liquid crystal gels. *Proc Natl Acad Sci USA* 2020;117:5125-33. DOI PubMed PMC
65. Wani OM, Zeng H, Priimagi A. A light-driven artificial flytrap. *Nat Commun* 2017;8:15546. DOI PubMed PMC
66. Pei Z, Yang Y, Chen Q, Terentjev EM, Wei Y, Ji Y. Mouldable liquid-crystalline elastomer actuators with exchangeable covalent bonds. *Nat Mater* 2014;13:36-41. DOI
67. Zou W, Dong J, Luo Y, Zhao Q, Xie T. Dynamic covalent polymer networks: from old chemistry to modern day innovations. *Adv Mater* 2017;29:1606100. DOI PubMed
68. Cui Y, Wang C, Sim K, et al. A simple analytical thermo-mechanical model for liquid crystal elastomer bilayer structures. *AIP Adv* 2018;8:025215. DOI
69. Cui Y, Yin Y, Wang C, et al. Transient thermo-mechanical analysis for bimorph soft robot based on thermally responsive liquid crystal elastomers. *Appl Math Mech Engl Ed* 2019;40:943-52. DOI
70. Guin T, Settle MJ, Kowalski BA, et al. Layered liquid crystal elastomer actuators. *Nat Commun* 2018;9:2531. DOI PubMed PMC
71. Ohm C, Fleischmann E, Kraus I, Serra C, Zentel R. Control of the properties of micrometer-sized actuators from liquid crystalline elastomers prepared in a microfluidic setup. *Adv Funct Mater* 2010;20:4314-22. DOI
72. de Jeu WH, Obraztsov EP, Ostrovskii BI, et al. Order and strain in main-chain smectic liquid-crystalline polymers and elastomers. *Eur Phys J E* 2008;25:117-8. DOI
73. Komp A, Finkelmann H. A new type of macroscopically oriented smectic-a liquid crystal elastomer. *Macromol Rapid Commun* 2007;28:55-62. DOI
74. Beyer P, Krueger M, Giesselmann F, Zentel R. Photoresponsive ferroelectric liquid-crystalline polymers. *Adv Funct Mater* 2007;17:109-14. DOI
75. Nishikawa E, Finkelmann H. Smectic-A liquid single crystal elastomers - strain induced break-down of smectic layers. Available from: https://onlinelibrary.wiley.com/doi/abs/10.1002/(SICI)1521-3935(19990201)200:2%3C312::AID-MACP312%3E3.0.CO;2-Y [Last accessed on 12 Apr 2023].
76. Thomsen DL, Keller P, Naciri J, et al. Liquid crystal elastomers with mechanical properties of a muscle. *Macromolecules* 2001;34:5868-75. DOI
77. Ahir S, Tajbakhsh A, Terentjev E. Self-assembled shape-memory fibers of triblock liquid-crystal polymers. *Adv Funct Mater* 2006;16:556-60. DOI
78. Soltani M, Raahemifar K, Nokhosteen A, Kashkooli FM, Zoudani EL. Numerical methods in studies of liquid crystal elastomers. *Polymers* 2021;13:1650. DOI PubMed PMC
79. Yang R, Zhao Y. Non-uniform optical inscription of actuation domains in a liquid crystal polymer of uniaxial orientation: an approach to complex and programmable shape changes. *Angew Chem Int Ed Engl* 2017;56:14202-6. DOI
80. Baumgartner M, Hartmann F, Drack M, et al. Resilient yet entirely degradable gelatin-based biogels for soft robots and electronics. *Nat Mater* 2020;19:1102-9. DOI
81. Ware TH, McConney ME, Wie JJ, Tondiglia VP, White TJ. Actuating materials. Voxelated liquid crystal elastomers. *Science* 2015;347:982-4. DOI PubMed
82. Konya A, Gimenez-pinto V, Selinger RLB. Modeling defects, shape evolution, and programmed auto-origami in liquid crystal elastomers. *Front Mater* 2016;3:24. DOI
83. McConney ME, Martinez A, Tondiglia VP, et al. Topography from topology: photoinduced surface features generated in liquid crystal polymer networks. *Adv Mater* 2013;25:5880-5. DOI
84. Xia Y, Zhang X, Yang S. Instant locking of molecular ordering in liquid crystal elastomers by oxygen-mediated thiol-acrylate click reactions. *Angew Chem Int Ed Engl* 2018;57:5665-8. DOI
85. Xia Y, Cedillo-Servin G, Kamien RD, Yang S. Guided folding of nematic liquid crystal elastomer sheets into 3D via patterned 1D microchannels. *Adv Mater* 2016;28:9637-43. DOI PubMed
86. Saed MO, Ambulo CP, Kim H, et al. Molecularly-engineered, 4D-printed liquid crystal elastomer actuators. *Adv Funct Mater* 2019;29:1806412. DOI
87. Jampani VSR, Mulder DJ, De Sousa KR, Gélébart A, Lagerwall JPF, Schenning APHJ. Micrometer-scale porous buckling shell actuators based on liquid crystal networks. *Adv Funct Mater* 2018;28:1801209. DOI
88. He Q, Wang Z, Wang Y, Song Z, Cai S. Recyclable and self-repairable fluid-driven liquid crystal elastomer actuator. *ACS Appl Mater Interf* 2020;12:35464-74. DOI
89. Zhai Y, Ng TN. Self-sustained robots based on functionally graded elastomeric actuators carrying up to 22 times their body weight. *Adv Intell Syst* 2021;[Accepted]:2100085. DOI
90. Ambulo CP, Burroughs JJ, Boothby JM, Kim H, Shankar MR, Ware TH. Four-dimensional printing of liquid crystal elastomers. *ACS Appl Mater Interf* 2017;9:37332-9. DOI PubMed
91. Ford MJ, Palaniswamy M, Ambulo CP, Ware TH, Majidi C. Size of liquid metal particles influences actuation properties of a liquid crystal elastomer composite. *Soft Matter* 2020;16:5878-85. DOI PubMed
92. Liu J, Gao Y, Wang H, Poling-skutvik R, Osuji CO, Yang S. Shaping and locomotion of soft robots using filament actuators made from liquid crystal elastomer-carbon nanotube composites. *Adv Intell Syst* 2020;2:1900163. DOI
93. Slavney AH, Hu T, Lindenberg AM, Karunadasa HI. A bismuth-halide double perovskite with long carrier recombination lifetime for photovoltaic applications. *J Am Chem Soc* 2016;138:2138-41. DOI PubMed

94. Wang M, Sayed SM, Guo L, et al. Multi-stimuli responsive carbon nanotube incorporated polysiloxane azobenzene liquid crystalline elastomer composites. *Macromolecules* 2016;49:663-71. DOI
95. Montazami R, Spillmann CM, Naciri J, Ratna BR. Enhanced thermomechanical properties of a nematic liquid crystal elastomer doped with gold nanoparticles. *Sens Actuator A Phys* 2012;178:175-8. DOI
96. Wójcik MM, Wróbel J, Jańczuk ZZ, et al. Liquid-crystalline elastomers with gold nanoparticle cross-linkers. *Chemistry* 2017;23:8912-20. DOI
97. Sun Y, Evans JS, Lee T, et al. Optical manipulation of shape-morphing elastomeric liquid crystal microparticles doped with gold nanocrystals. *Appl Phys Lett* 2012;100:241901. DOI
98. Zhang J, Wang J, Zhao L, et al. Photo responsive silver nanoparticles incorporated liquid crystalline elastomer nanocomposites based on surface plasmon resonance. *Chem Res Chin Univ* 2017;33:839-46. DOI
99. Guo LX, Liu MH, Sayed SM, et al. A calamitic mesogenic near-infrared absorbing croconaine dye/liquid crystalline elastomer composite. *Chem Sci* 2016;7:4400-6. DOI PubMed PMC
100. Liu L, Liu MH, Deng LL, Lin BP, Yang H. Near-infrared chromophore functionalized soft actuator with ultrafast photoresponsive speed and superior mechanical property. *J Am Chem Soc* 2017;139:11333-6. DOI PubMed
101. Qin B, Yang W, Xu J, et al. Photo-actuation of liquid crystalline elastomer materials doped with visible absorber dyes under quasi-daylight. *Polymers* 2019;12:54. DOI PubMed PMC
102. Zuo B, Wang M, Lin B, Yang H. Photomodulated tricolor-changing artificial flowers. *Chem Mater* 2018;30:8079-88. DOI
103. Huang Z, Tsui GC, Deng Y, et al. Bioinspired near-infrared light-induced ultrafast soft actuators with tunable deformation and motion based on conjugated polymers/liquid crystal elastomers. *J Mater Chem C* 2022;10:12731-40. DOI
104. Liu W, Guo L, Lin B, Zhang X, Sun Y, Yang H. Near-infrared responsive liquid crystalline elastomers containing photothermal conjugated polymers. *Macromolecules* 2016;49:4023-30. DOI
105. Hussain M, Jull EIL, Mandle RJ, Raistrick T, Hine PJ, Gleeson HF. Liquid crystal elastomers for biological applications. *Nanomaterials* 2021;11:813. DOI PubMed PMC
106. Dong L, Zhao Y. Photothermally driven liquid crystal polymer actuators. *Mater Chem Front* 2018;2:1932-43. DOI
107. Hauser AW, Liu D, Bryson KC, Hayward RC, Broer DJ. Reconfiguring nanocomposite liquid crystal polymer films with visible light. *Macromolecules* 2016;49:1575-81. DOI
108. Sánchez-Ferrer A, Merekalov A, Finkelmann H. Opto-mechanical effect in photoactive nematic side-chain liquid-crystalline elastomers. *Macromol Rapid Commun* 2011;32:671-8. DOI PubMed
109. Liu D, Liu L, Onck PR, Broer DJ. Reverse switching of surface roughness in a self-organized polydomain liquid crystal coating. *Proc Natl Acad Sci USA* 2015;112:3880-5. DOI PubMed PMC
110. Zeng H, Wasylczyk P, Wiersma DS, Priimagi A. Light robots: bridging the gap between microrobotics and photomechanics in soft materials. *Adv Mater* 2018;30:e1703554. DOI PubMed
111. Gelebart AH, Mc Bride M, Schenning APHJ, Bowman CN, Broer DJ. Photoresponsive fiber array: toward mimicking the collective motion of cilia for transport applications. *Adv Funct Mater* 2016;26:5322-7. DOI
112. Yu Y, Maeda T, Mamiya J, Ikeda T. Photomechanical effects of ferroelectric liquid-crystalline elastomers containing azobenzene chromophores. *Angew Chem Int Ed Engl* 2007;46:881-3. DOI PubMed
113. Palagi S, Mark AG, Reigh SY, et al. Structured light enables biomimetic swimming and versatile locomotion of photoresponsive soft microrobots. *Nat Mater* 2016;15:647-53. DOI
114. Rogóż M, Zeng H, Xuan C, Wiersma DS, Wasylczyk P. Light-driven soft robot mimics caterpillar locomotion in natural scale. *Adv Opt Mater* 2016;4:1689-94. DOI
115. Guo Y, Liu N, Cao Q, et al. Photothermal diol for NIR-responsive liquid crystal elastomers. *ACS Appl Polym Mater* 2022;4:6202-10. DOI
116. Yamada M, Kondo M, Miyasato R, et al. Photomobile polymer materials - various three-dimensional movements. *J Mater Chem* 2009;19:60-2. DOI
117. Schuhladen S, Preller F, Rix R, Petsch S, Zentel R, Zappe H. Iris-like tunable aperture employing liquid-crystal elastomers. *Adv Mater* 2014;26:7247-51. DOI PubMed
118. Fowler HE, Rothemund P, Keplinger C, White TJ. Liquid crystal elastomers with enhanced directional actuation to electric fields. *Adv Mater* 2021;33:e2103806. DOI PubMed
119. Gu G, Zou J, Zhao R, Zhao X, Zhu X. Soft wall-climbing robots. *Sci Robot* 2018;3:eaat2874. DOI
120. Chambers M, Finkelmann H, Remškar M, Sánchez-ferrer A, Zalar B, Žumer S. Liquid crystal elastomer-nanoparticle systems for actuation. *J Mater Chem* 2009;19:1524-31. DOI
121. Papadopoulos P, Heinze P, Finkelmann H, Kremer F. Electromechanical properties of smectic C* liquid crystal elastomers under shear. *Macromolecules* 2010;43:6666-70. DOI
122. Ambulo CP, Ford MJ, Searles K, Majidi C, Ware TH. 4D-printable liquid metal-liquid crystal elastomer composites. *ACS Appl Mater Interf* 2021;13:12805-13. DOI PubMed
123. Kotikian A, Morales JM, Lu A, et al. Innervated, self-sensing liquid crystal elastomer actuators with closed loop control. *Adv Mater* 2021;33:e2101814. DOI
124. Zhang R, Redford SA, Ruijgrok PV, et al. Spatiotemporal control of liquid crystal structure and dynamics through activity patterning. *Nat Mater* 2021;20:875-82. DOI PubMed PMC

125. Ford MJ, Ambulo CP, Kent TA, et al. A multifunctional shape-morphing elastomer with liquid metal inclusions. *Proc Natl Acad Sci USA* 2019;116:21438-44. DOI PubMed PMC
126. Davidson ZS, Shahsavan H, Aghakhani A, et al. Monolithic shape-programmable dielectric liquid crystal elastomer actuators. *Sci Adv* 2019;5:eaay0855. DOI PubMed PMC
127. Harris KD, Bastiaansen CW, Lub J, Broer DJ. Self-assembled polymer films for controlled agent-driven motion. *Nano Lett* 2005;5:1857-60. DOI PubMed
128. Haan LT, Verjans JM, Broer DJ, Bastiaansen CW, Schenning AP. Humidity-responsive liquid crystalline polymer actuators with an asymmetry in the molecular trigger that bend, fold, and curl. *J Am Chem Soc* 2014;136:10585-8. DOI
129. Abadia AV, Herbert KM, White TJ, Schwartz DK, Kaar JL. Biocatalytic 3D actuation in liquid crystal elastomers via enzyme patterning. *ACS Appl Mater Interf* ;2022:26480-8. DOI
130. Michal BT, Mckenzie BM, Felder SE, Rowan SJ. Metallo-, thermo-, and photoresponsive shape memory and actuating liquid crystalline elastomers. *Macromolecules* 2015;48:3239-46. DOI
131. Harris KD, Bastiaansen CWM, Broer DJ. Physical properties of anisotropically swelling hydrogen-bonded liquid crystal polymer actuators. *J Microelectromech Syst* 2007;16:480-8. DOI
132. Boothby JM, Kim H, Ware TH. Shape changes in chemoresponsive liquid crystal elastomers. *Sens Actuators B Chem* 2017;240:511-8. DOI
133. Zhang J, Guo Y, Hu W, Soon RH, Davidson ZS, Sitti M. Liquid crystal elastomer-based magnetic composite films for reconfigurable shape-morphing soft miniature machines. *Adv Mater* 2021;33:e2006191. DOI
134. Herrera-Posada S, Mora-Navarro C, Ortiz-Bermudez P, et al. Magneto-responsive liquid crystalline elastomer nanocomposites as potential candidates for dynamic cell culture substrates. *Mater Sci Eng C Mater Biol Appl* 2016;65:369-78. DOI
135. Zhang J, Guo Y, Hu W, Sitti M. Wirelessly actuated thermo- and magneto-responsive soft bimorph materials with programmable shape-morphing. *Adv Mater* 2021;33:e2100336. DOI
136. Zeng H, Wani OM, Wasylczyk P, Priimagi A. Light-driven, caterpillar-inspired miniature inching robot. *Macromol Rapid Commun* 2018;39:1700224. DOI PubMed
137. Rogóż M, Dradrach K, Xuan C, Wasylczyk P. A millimeter-scale snail robot based on a light-powered liquid crystal elastomer continuous actuator. *Macromol Rapid Commun* 2019;40:e1900279. DOI PubMed
138. Zeng H, Wasylczyk P, Parmeggiani C, Martella D, Burresi M, Wiersma DS. Light-fueled microscopic walkers. *Adv Mater* 2015;27:3883-7. DOI PubMed PMC
139. Hu J, Nie Z, Wang M, Liu Z, Huang S, Yang H. Springtail-inspired light-driven soft jumping robots based on liquid crystal elastomers with monolithic three-leaf panel fold structure. *Angew Chem Int Ed Engl* 2023;62:e202218227. DOI
140. Zhao Y, Hong Y, Qi F, Chi Y, Su H, Yin J. Self-sustained snapping drives autonomous dancing and motion in free-standing wavy rings. *Adv Mater* 2023;35:e2207372. DOI
141. Martella D, Nocentini S, Nuzhdin D, Parmeggiani C, Wiersma DS. Photonic microhand with autonomous action. *Adv Mater* 2017;29:1704047. DOI PubMed
142. Huang Y, Bisoyi HK, Huang S, et al. Bioinspired synergistic photochromic luminescence and programmable liquid crystal actuators. *Angew Chem Int Ed Engl* 2021;60:11247-51. DOI
143. Lyu P, Astam MO, Sánchez-somolinos C, Liu D. Robotic pick-and-place operations in multifunctional liquid crystal elastomers. *Adv Intell Syst* 2022;4:2200280. DOI
144. Potekhina A, Wang C. Liquid crystal elastomer based thermal microactuators and photothermal microgrippers using lateral bending beams. *Adv Mater Technol* 2022;7:2101732. DOI
145. Tian H, Liu H, Shao J, Li S, Li X, Chen X. An electrically active gecko-effect soft gripper under a low voltage by mimicking gecko's adhesive structures and toe muscles. *Soft Matter* 2020;16:5599-608. DOI
146. De Bellis I, Ni B, Martella D, et al. Color modulation in morpho butterfly wings using liquid crystalline elastomers. *Adv Intell Syst* 2020;2:2000035. DOI
147. Shi Y, Zhu C, Li J, Wei J, Guo J. A color-changing plasmonic actuator based on silver nanoparticle array/liquid crystalline elastomer nanocomposites. *New J Chem* 2016;40:7311-9. DOI
148. Zhang P, de Haan LT, Debije MG, Schenning APHJ. Liquid crystal-based structural color actuators. *Light Sci Appl* 2022;11:248. DOI PubMed PMC
149. Liu Z, Bisoyi HK, Huang Y, Wang M, Yang H, Li Q. Thermo- and mechanochromic camouflage and self-healing in biomimetic soft actuators based on liquid crystal elastomers. *Angew Chem Int Ed Engl* 2022;61:e202115755. DOI
150. Joralmon D, Alfarhan S, Kim S, Tang T, Jin K, Li X. Three-dimensional printing of liquid crystals with thermal sensing capability via multimaterial vat photopolymerization. *ACS Appl Polym Mater* 2022;4:2951-9. DOI
151. Wei W, Gao J, Yang J, Wei J, Guo J. A NIR light-triggered pyroelectric-dominated generator based on a liquid crystal elastomer composite actuator for photoelectric conversion and self-powered sensing. *RSC Adv* 2018;8:40856-65. DOI PubMed PMC
152. Liao W, Yang Z. The integration of sensing and actuating based on a simple design fiber actuator towards intelligent soft robots. *Adv Mater Technol* 2022;7:2101260. DOI
153. Shaha RK, Merkel DR, Anderson MP, et al. Biocompatible liquid-crystal elastomers mimic the intervertebral disc. *J Mech Behav Biomed Mater* 2020;107:103757. DOI
154. Hussain S, Park SY. Photonic cholesteric liquid-crystal elastomers with reprogrammable helical pitch and handedness. *ACS Appl*

*Mater Interf* 2021;13:59275-87. DOI PubMed

155. Frenzel T, Köpfler J, Jung E, Kadic M, Wegener M. Ultrasound experiments on acoustical activity in chiral mechanical metamaterials. *Nat Commun* 2019;10:3384. DOI PubMed PMC

156. Yan D, Chang J, Zhang H, et al. Soft three-dimensional network materials with rational bio-mimetic designs. *Nat Commun* 2020;11:1180. DOI PubMed PMC

157. Xue Z, Jin T, Xu S, et al. Assembly of complex 3D structures and electronics on curved surfaces. *Sci Adv* 2022;8:eabm6922. DOI PubMed PMC